A TRU-Zr METAL-FUEL SODIUM-COOLED FAST SUBCRITICAL ADVANCED BURNER REACTOR

FUEL CYCLE AND MANAGEMENT

KEYWORDS: *advanced burner reactor, transmutation fuel cycle, sodium fast reactor*

W. M. STACEY,* W. VAN ROOIJEN, T. BATES, E. COLVIN, J. DION, J. FEENER, E. GAYTON, D. GIBBS, C. GRENNOR, J. HEAD, F. HOPE, J. IRELAND, A. JOHNSON, B. JONES, N. MEJIAS, C. MYERS, A. SCHMITZ, C. SOMMER, T. SUMNER, and L. TSCHAEPE *Georgia Institute of Technology*
Nuclear and Radiological Engineering Program, Atlanta, Georgia 30332-0425

Received May 29, 2007
Accepted for Publication October 4, 2007

The design concept of a subcritical advanced burner reactor (SABR) is described. SABR is fueled with transuranics (TRUs) discharged from thermal reactors cast into a TRU-Zr metal fuel pin and is cooled with sodium. The reactor operates subcritical to achieve a deep-burn four-batch fuel cycle that fissions 25% of the TRU in an 8.2-yr residence time, limited by radiation damage accumulation (200 displacements per atom) in the oxygen dispersion strengthened clad and structure. The annual TRU fission rate in SABR [3000 MW(thermal)] is comparable to the annual TRU discharge of three to five 1000-MW(electric) light water reactors, depending on the plant capacity factor of SABR. A tokamak D-T fusion neutron source based on physics and technology that will be demonstrated in ITER supports the subcritical operation.

I. INTRODUCTION

Closing the nuclear fuel cycle is the major technical challenge to the expansion of nuclear energy to meet the world's growing need for environmentally benign electrical power for the remainder of the century. The U.S. Department of Energy (DOE) Global Nuclear Energy Partnership[1] (GNEP) and Generation IV Initiative[2] (GEN-IV) are addressing this challenge by developing the nuclear technology to minimize the long-lived transuranics (TRUs) in spent nuclear fuel (SNF) that must be stored in high-level waste repositories (HLWR) and to better utilize the potential energy content of the uranium fuel resource. Specifically, the GNEP will develop a consolidated fuel treatment center for separating the TRUs from the SNF discharged by light water reactors (LWRs) to use as fuel in an advanced burner reactor (ABR). The GEN-IV effort is focusing on fast reactors that will be able to transmute the nonfissionable ^{238}U (99.3% of natural uranium) into fissionable TRU isotopes (and on other advanced reactors for other missions).

The concept of separating the TRUs in SNF discharged from LWRs and using it as fuel in fast (and thermal) reactors, with the primary motivation of reducing the long-lived radioactive TRU isotopes in the waste sent to HLWRs, was extensively investigated[3–6] in the 1990s. The general conclusion of these investigations was that, by repeatedly reprocessing the fuel and recycling the remaining TRU, the TRU in the waste ultimately sent to HLWRs could be reduced by a large factor ($>$90%). Another conclusion was that the use of subcritical reactors that could operate with highly burned fuel or with fuel consisting of the minor actinides (Am, Cm) would be necessary to achieve $\gg$90% burnup of the TRU.

Several conceptual designs and fuel cycle analyses of subcritical transmutation reactors with an accelerator-spallation neutron source[3–6] were investigated during the 1990s. Subsequently, a series of conceptual designs and fuel cycle analyses of subcritical fast transmutation reactors with tokamak D-T fusion neutron sources were developed at Georgia Institute of Technology.[7–12] A general conclusion of these studies was that subcritical operation provides much greater fuel cycle flexibility to achieve "deep burn" of a large quantity of TRU, hence to significantly (i.e., by one to two orders of magnitude) reduce the HLWR requirements.

*E-mail: weston.stacey@nre.gatech.edu

Our initial fast reactor design[7] with a fusion neutron source was based on the metal-fuel sodium-cooled and lead-bismuth–cooled fast reactor designs[13,14] that had been developed for the transmutation reactor design with an accelerator neutron source, but with a lead-lithium coolant in order also to achieve tritium breeding. Then, a series of helium-cooled TRU-fueled fast reactor designs[8–10] were carried out to investigate the prospects for achieving deep burnup of the TRU in TRISO fuel particles that then could be placed in the HLWR without further reprocessing.

Now, with the GNEP emphasis on early deployment of an ABR, the conceptual design of a TRU metal-fuel sodium-cooled fast subcritical ABR (SABR) with a tokamak D-T fusion neutron source is proposed, in order to take advantage of the added flexibility for achieving deep burnup of the TRU provided by subcritical operation. Since the fusion neutron source design[15] is based on the physics and technology that has been developed for and that will be demonstrated in the International Thermonuclear Experimental Reactor[16] (ITER), which will begin operation in 2017, the SABR is proposed as a possible second-generation ABR.

II. DESIGN OVERVIEW

II.A. Configuration and Dimensions

The SABR is a subcritical metal-fueled sodium-cooled fast reactor driven by a tokamak D-T fusion neutron source. A simplified three-dimensional (3-D) view of the design is shown in Fig. 1. The annular fission core surrounds the fusion neutron source on the outboard side. The fission core and the plasma are surrounded first by a combination of reflector and tritium-breeding blanket, then by a shield; the combined thickness of these materials is 80 cm. Items not shown in Fig. 1 include the divertor below the plasma, an emergency core cooling system above the core, coolant flow pipes, control rod drives above the core, and other systems that were not developed in detail.

The primary objective of SABR is to transmute the TRUs in SNF in order to reduce HLWR requirements. In the process, power will be produced that will be converted to electricity. In order to reach this secondary objective, a three-loop cooling system is employed with sodium as the primary and intermediate coolant. The secondary loop, with water as the working fluid in a Rankine cycle, will employ high-pressure and low-pressure turbines to produce power.

The 3.2-m core height shown in Fig. 1 corresponds to the 2-m active length of the fuel, a 1-m gas plenum, and a 20-cm reflector included within the fuel rod to reduce neutron leakage into the plenum. The fuel pin is a 4-mm-diam metallic TRU-Zr slug, clad in ODS steel with a sodium bond. The outer diameter of the fuel pin is 7.26 mm. The reactor core consists of 918 hexagonal fuel assemblies, each containing 271 fuel pins. Sixteen assemblies contain enriched boron carbide control rods.

Figure 2, which is the model used for neutronics calculations, shows the detailed dimensions of the reactor. This model simplifies the actual geometry above and below the core and plasma. For example, the shield configuration must allow for a divertor below the plasma and control rod drives above the core. As seen in Fig. 2, the fission core is divided into four regions, each with an equal number of assemblies (for fuel shuffling). The detailed layout of the assemblies and the batch arrangement is shown in Fig. 3. Every 750 days, the most burned batch

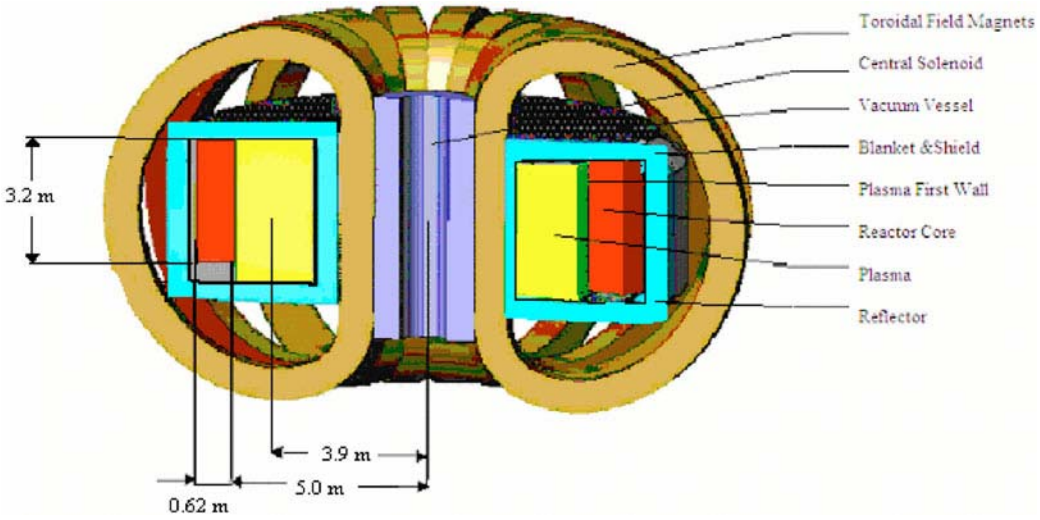

Fig. 1. Configuration of the SABR.

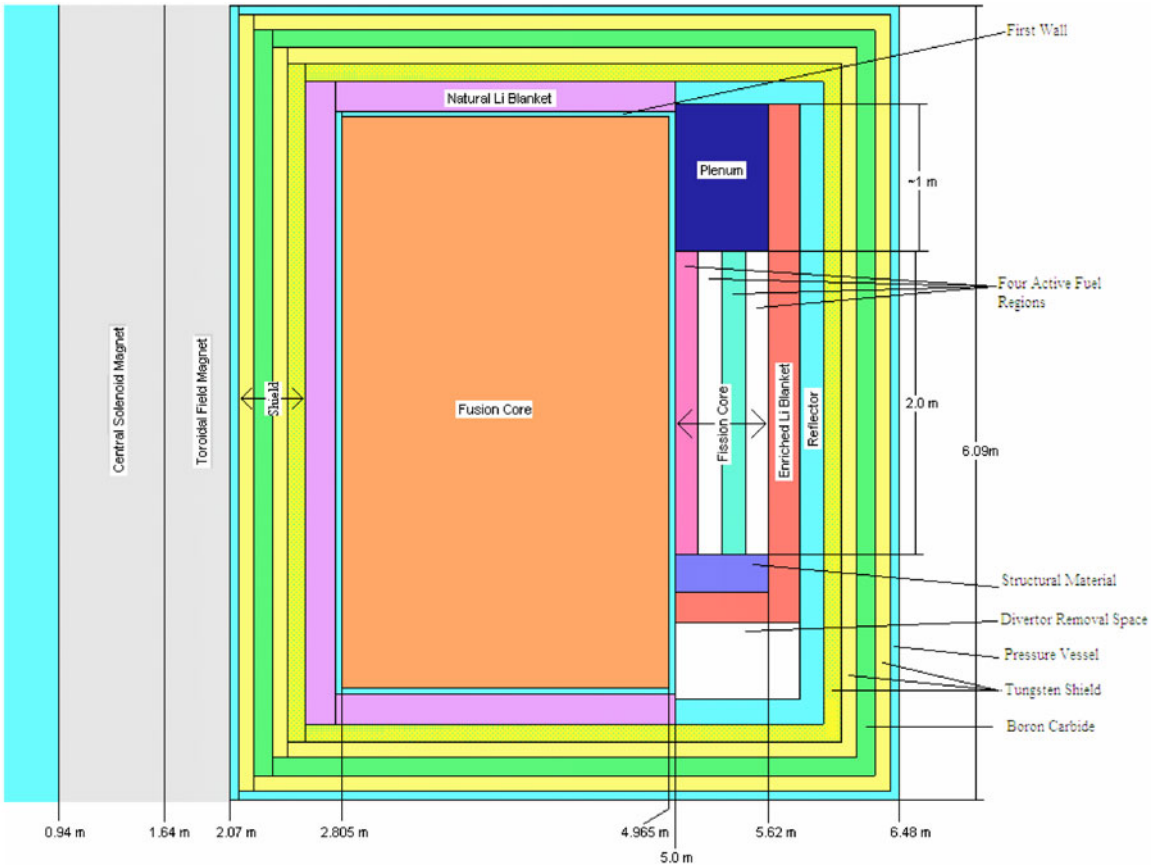

Fig. 2. Cross section of the SABR calculation model.

will be discharged, a fresh batch will be added, and the remaining assemblies will be moved.

The design for the toroidal tokamak neutron source is taken from a previous design[9,10] and is a scaled-down version of the ITER design.[16] The height of the plasma chamber is 3.76 m, and the width is 2.16 m. A divertor (not shown) is located below the plasma chamber. Sixteen "D-shaped" superconducting toroidal field magnets surround the reactor. Each magnet is 5.4 m in horizontal bore and 8.4 m in vertical bore, with radial thickness of 43 cm and toroidal thickness of 36 cm. This leaves ~1 m of free space for access between the shield and the magnets on the top and outboard. The superconducting central solenoid magnet has an inner radius of 94 cm and a thickness of 70 cm.

II.B. Major Parameters and Materials

Table I gives a summary of the major parameters and materials used in the SABR design. The isotopic composition of the TRU fuel is given later. All other materials are commercially available items. Unless otherwise noted, all structural material is oxygen dispersion strengthened (ODS) (MA957) steel.

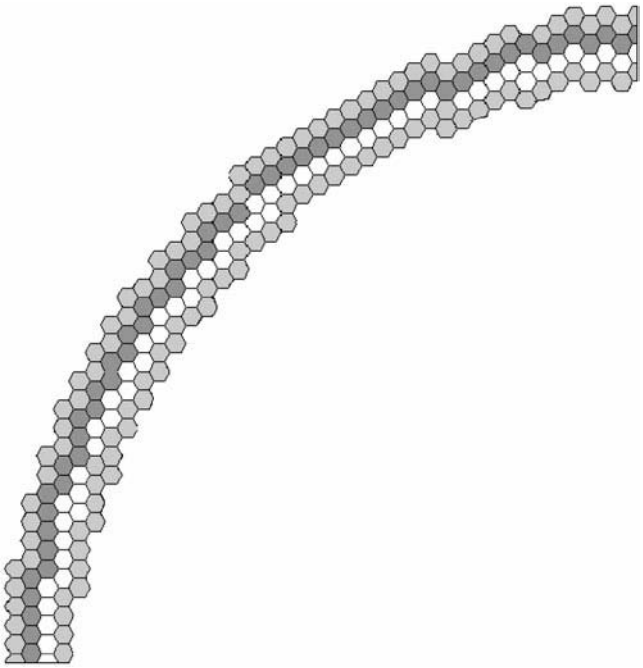

Fig. 3. Four-batch layout of fuel assemblies.

TABLE I

Major Parameters and Materials of the SABR

Fission core	
Fission power	3000 MW(thermal)
TRU fuel composition (wt%)	40Zr-10Am-10Np-40Pu
Fuel density	9.595 g/cm^3
Mass of TRU/fuel material	36 t/60 t
Specific power	83.3 kW(thermal)/kg TRU
Maximum k_{eff}	0.95
Major dimensions	R_{in} = 5 m, R_{out} = 5.62 m, H_{active} = 2 m
Fuel pin	Number = 248 778, D_{fm} = 4.00 mm, D_o = 7.26 mm
Coolant mass flow rate, temperature	$\dot{m}$ = 8700 kg/s, T_{in}/T_{out} = 377/650°C
Power density, maximum T_{fuel}/T_{clad}	q''' = 72.5 MW/m^3, $T_{fm,\max}$ = 715°C, $T_{clad,\max}$ = 660°C
Linear fuel pin power	6 kW/m
Clad, wire wrap, and flow tube	ODS ferritic steel, t = 0.5, 2.2, 2.0 mm
Fuel/clad, gap, $LiNbO_3$/structure/coolant (vol%)	15/35/14/36
Fuel assembly	Number = 918, hex, D_{flats} = 15.5 cm, D_{side} = 8.95 cm
Reflector, blanket, and shield	
Reflector/shield materials	ODS steel, boron carbide, tungsten, Na cooled
Tritium breeder	Li_2SiO_4
Combined thickness	80 cm
Tritium breeding ratio	1.16
Coolant mass flow rate	$\dot{m}$ = 0.2 kg/s
Minimum and maximum blanket temperatures	$T_{\min}$ = 450°C/$T_{\max}$ = 640°C
Plasma	
Plasma current	8 to 10.0 MA
Fusion power/neutron source rate	(50 to 500 MW)/(1.8×10^{19} to 1.8×10^{20} s^{-1})
Fusion gain ($Q_p = P_{fus}/P_{plasma\ heating}$)	180 MW(thermal)/58 MW(thermal) = 3.2
Superconducting magnets	
Field central solenoid, toroidal field coil, at center of plasma	13.5 T, 11.8 T, 5.9 T
Toroidal field coil magnet dimensions	w = 5.4 m, h = 8.4 m, t_{rad} = 43 cm, t_{tor} = 36 cm
Divertor	
Materials	Tungsten, CuCrZr, Na cooled
Heat flux	1 to 8 MW/m^2
Coolant mass flow rate	$\dot{m}$ = 0.09 kg/s
First wall	
Materials	Beryllium on ODS, Na cooled
Surface area	223 m^2
Average neutron wall load (14 MeV)	1.0 MW/m^2
Average heat flux (500 MW)	0.25 MW/m^2
Coolant mass flow rate	$\dot{m}$ = 0.057 kg/s

II.C. Calculation of Fuel Loading

The SABR is designed to be operated as a subcritical source-driven reactor, and the maximum value of k_{eff}, which will occur for initial startup with fresh TRU fuel in all assemblies, is specified to be no more than 0.95. To determine the amount of fuel necessary to achieve this multiplication, the core was modeled using the 3-D continuous-energy Monte Carlo code MCNP (Ref. 17), with temperature-corrected cross sections generated with NJOY (Ref. 18) from ENDF/B-VI.6 and ENDF/B-VII libraries.[19] Using the core dimensions in Table I, it was determined that 36 t of TRUs (60 t of 40Zr-10Am-10Np-40Pu fuel) was necessary to achieve k_{eff} = 0.95 for all fresh fuel. The reactivity decrease due to fuel burnup will be compensated by increasing the neutron source.

II.D. Fabrication and Reprocessing

The fuel will be fabricated through arc casting and will be reprocessed using pyrometallurgical reprocessing. A single arc-casting facility can annually fabricate approximately 60 581 fuel pins containing a total of

8760 kg of TRU. Pyroprocessing is based on the use of high-temperature fused chloride salts to melt the fuel, along with electrorefining techniques to separate the TRUs and fission products. Pyroprocessing is specifically suited for metallic fuels. A key benefit of pyroprocessing is that the actinides are never separated individually, but are instead recycled as one group, making them highly proliferation resistant.

II.E. Component Lifetime

The length of time that the reactor can operate continuously is determined by the expected time-to-failure of the various components. Interactions with fast (>0.1 MeV) neutrons cause atomic displacements, transmutation of atoms, and hydrogen and helium gas production within the fuel pin and other components. These damaging effects determine how long essential reactor components such as cladding, fuel, first wall, and magnets can remain in operation. Using a damage limit of 200 displacements per atom (dpa) for ODS steel, the radiation damage lifetime of the clad and fuel assembly structure is found to be somewhat more than 8 yr. This places an upper limit of 3000 days on the fuel residence time. The first wall is found to have a radiation damage lifetime of somewhat more than 8 yr. Therefore, it will have to be replaced several times over the life of the reactor. The shield is designed so that the magnets will not have to be replaced during the lifetime of the reactor.

II.F. Transmutation, Electrical, and Safety Performance

As mentioned previously, the primary purpose of the SABR is to burn the TRUs produced by LWRs to reduce the requirements for HLWRs. The SABR is successful in this goal as it achieves a transmutation rate of 1.06 t of TRU per full power year. The annual production of SNF in the United States is ~2000 t U/yr (Ref. 6) for ~100 000 MW(electric). Of this, only 1% is TRUs (Ref. 20). This means that, on average, one 1000-MW(electric) LWR discharges 0.2 t of TRU per year. The support ratio for SABR is determined by the transmutation rate and the availability of the reactor. At 100% (60%) availability the SABR can burn the TRU discharged annually from five (three) 1000-MW(electric) LWRs.

The SABR fission core produces 3000-MW(thermal) power. The gross power produced by the turbine in the final loop is 1049 MW(electric). Some of this power will be reused by the system to power supporting systems, such as the coolant flow pumps and plasma heating source. The power required to operate the fusion neutron source is 90 MW(electric) (Ref. 10). Total power required to run all pumps in the system is 7.65 MW(electric). Heaters take up an additional 30 MW(electric) on a Rankine cycle. Therefore, the net electrical power produced is 921 MW(electric). This corresponds to a 30.7% net efficiency for the plant (conversion efficiency was not a design priority, and this value could certainly be increased).

Dynamic simulations indicate that accidental reduction in coolant flow by up to approximately two-thirds could be passively tolerated without sodium boiling or fuel melting and that tens of seconds would be available to prevent sodium boiling or fuel melting by control action—neutron source termination or control rod insertion—for larger reductions in coolant flow.

III. FUELS

III.A. Metal TRU Fuel

Fuel candidates for transmutation reactor design can be divided into two groups based upon the type of reprocessing that they require. The first group consists of oxide, nitride, and carbide fuel types that are reprocessed using aqueous methods. The second group consists solely of metal fuels that are reprocessed using pyrometallurgic processes. The decision for fuel type was therefore contingent on both fuel type and reprocessing method. Current research in the United States for transmutation reactor designs with high minor actinide content indicates that the nitride and metal-based fuel elements are the frontrunners.[21] Therefore, only nitride and metal fuels were considered for use in the SABR. Nitride fuels have been successfully irradiated up to 5.5% burnup in JMTR (Ref. 22), while metal fuels have been successfully irradiated up to ~20% in EBR-II (Ref. 23). Both candidates show excellent fission gas retention,[21,22] and both have excellent thermal conductivities.[22,24]

A major factor in the fuel choice decision was that the aqueous reprocessing associated with nitride fuel was determined to be inferior to pyroprocessing. The two main advantages of pyroprocessing are that the process is proliferation resistant and can be accomplished with an on-site facility, which reduces the costs and associated risks of transporting the spent fuel from the reactor.[25] The disadvantages associated with using aqueous reprocessing methods include large amounts of high activity fission product-bearing aqueous and nonaqueous wastes, the necessity of large production sites and production-scale equipment, and proliferation concerns due to the ability of the process to generate highly purified and separate uranium and plutonium.[23] Also, there are recovery issues concerning ^{15}N-enriched gas when using aqueous reprocessing with nitride fuel.[22]

Metal TRU-Zr fuel is proposed for the liquid sodium–cooled SABR. The fuel will have a weight percent composition of 40Zr-10Am-10Np-40Pu. This fuel type was chosen because it is currently being developed at Argonne National Laboratory (ANL) for use in the U.S. advanced fuel cycle initiative.[24] In general, metal fuel has properties that prove favorable for applications with priority of high burnup of TRU, including high thermal

conductivity, the ability to accommodate a high actinide density, and the ability to be directly fed into pyroprocessing and refabrication facilities.[21]

Zirconium is selected as the alloying element because it has been successfully fabricated and reprocessed. In addition, metal fuel dispersed in a zirconium matrix has demonstrated excellent radiation resistance.[26] The inclusion of zirconium in the metal composition raises the alloy solidus temperature, provides resistance between clad and fuel interactions,[27] provides dimensional stability during irradiation,[28] and provides the possibility of a negative Doppler coefficient in TRU fuel that is free of ^{238}U.

III.B. ODS Steel Cladding

Both ferretic and ODS ferretic steel were considered for the cladding material. ODS ferretic steel was favored on the basis that ODS steels are mechanically superior, have much better resistance to thermal creep at higher temperatures, and are compatible with both the fuel and liquid sodium.[29–31] MA957, a mechanically alloyed and commercially available ODS steel developed by INCO Metals, was chosen for the reference cladding material. Several experimental ODS steels undergoing development may show better mechanical properties than MA957 (Table II); however, at the present time, MA957 has endured a much more comprehensive battery of tests for suitability in a fast reactor setting.[32,33]

III.C. Fuel Element Design

The fuel pin design is determined by the requirement to provide enough fuel to enable SABR to produce 3000 MW(thermal) over a four-batch burn cycle and by the thermal and structural limitations of the materials. To aid in the choices of pin design, similar reactors with sodium-cooled metal-fuel designs such as the HYPER (Ref. 34), JAERI (Ref. 35), and ALMR (Ref. 36) were reviewed. The dimensions were chosen such that the operating temperature of the clad should not exceed 700°C anywhere in the core. Temperatures above this point in stainless steels have been found experimentally to have unacceptable stresses caused by fuel swelling and fission gas buildup.[37] Fuel swelling and fission gas buildup must be accounted for to prevent the clad from expanding or rupturing. Coolant flow area must be large enough to cool the core and keep velocity below 8 m/s to prevent structural vibration.[37]

TABLE II

Properties of MA957

Density	7.3 g/cm^3 (300 K)
Melting point	1800 K
Recrystallization temperature	1620 K
Ductile to brittle transformation	220 to 330 K
Linear coefficient of thermal expansion	1.4×10^{-5}/K (650°C)
Thermal conductivity	20 W/m K (650°C)
Specific heat	600 J/kg K (650°C)
Composition by weight percent: 84.55Fe-14Cr-0.9Ti-0.3Mo-0.25Y_2O_3	

The starting point of the design was the fuel choice of 40Zr-10Am-10Np-40Pu (wt%), which is being developed at ANL. The ANL reports[21] used a 4-mm-diam fuel pin and a 0.455-mm clad thickness. As a result, this was chosen to be the diameter of the fuel material in this design. The clad thickness was increased slightly to 0.5 mm. This value is within the range of values used for JAERI (Ref. 35) (0.3-mm ODS), ALMR (Ref. 36) (0.5-mm HT9), and HYPER (Ref. 34) (0.7-mm HT9). Neutronics calculations discussed in Sec. IV were made to determine the amount of fresh fuel needed for a k_{eff} of 0.95. These calculations combined with the constraints listed above led to an active fuel length choice of 2.0 m. This gives a modest linear power density of 6 kW/m (45 kW/m is more typical of fast reactors).

A critical issue that is linked with transmutation fuels is the high helium generation rates due to the alpha decay of ^{241}Am. This helium gas production substantially increases the plenum requirements of the fuel pin and can cause substantial fuel swelling.[21] The fission gas plenum for this reactor is based on the findings of the Korean HYPER design. With a similar TRU fuel and clad thickness, it was found that the cladding strain values are 3.3, 3.1, and 3.01% at 30 at.% burnup for the 0.5, 1.0, and 1.5 plenum-to-fuel ratios, respectively.[38] The limiting value of the strain is normally taken to be 3.0% for HT9 steel.[38] Therefore, it is recommended that a 1.5 plenum-to-fuel ratio is used. ODS steels, however, are expected to outperform HT9 in fast reactors at high temperatures. In view of the fact that the strain values vary only slightly between the cases and that increasing the dimensions comes with such a high cost, this design will use a modest plenum-to-fuel ratio of 1.0. This corresponds to a 1.0-m plenum on top of the core. The plenum is initially vacant space and gradually becomes filled with gas as the fuel is irradiated.

Nuclear fuel swells as it is fissioned because of the quantum mechanical nature of atoms occupying approximately the same volume (10^{-29} m^2) regardless of mass.[37] To allow room for fuel expansion due to solid fission products, a large fuel to clad gap size is designed for beginning of life. A typical design is for the fuel to occupy 75% of the cross-sectional area of the interior tube.[21] This allows the fuel volume to increase by ~30% before coming into contact with the clad. However, for this reactor, the gap size is nearly doubled to be conservative. This also allows the gas plenum volume to be larger with minimal length. The gap is filled with sodium, instead of helium, to increase conductivity across the gap. This is

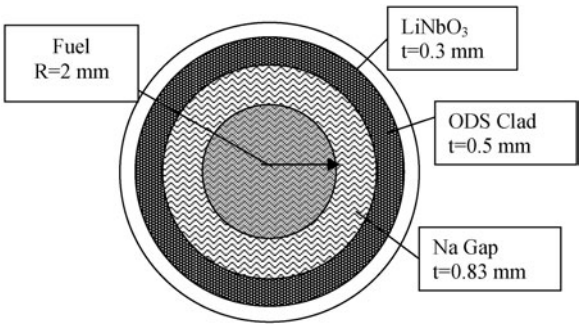

Fig. 4. Cross-sectional view of fuel.

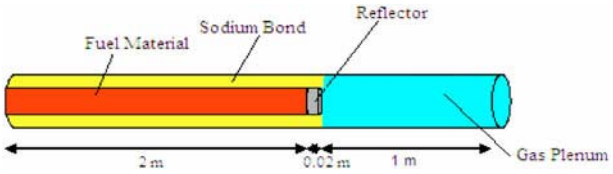

Fig. 5. Axial view of fuel pin.

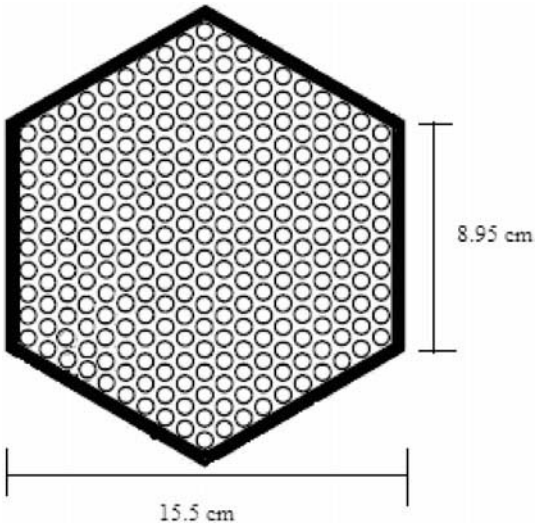

Fig. 6. Cross-sectional view of fuel assembly.

necessary because of the high coolant outlet temperature and the relatively low melting temperature of the fuel. If a helium gap can be used, it would not be necessary to have the 1-m-long fission plenum above the rods, as the gases would be free to fill the radial gap space. Ultimately, the design decision is a tradeoff that must be optimized depending on the specific design objectives. The actual amount of fuel expansion cannot be determined without experiments, but this design is expected to be conservative. The fuel pin design parameters are given in Figs. 4 and 5 and in Table III.

The fuel rods are arranged into 918 hexagonal fuel assemblies with 271 rods per assembly (Fig. 6). Assemblies are fully wrapped with 2-mm-thick ODS steel. Rods are held in place and prevented from bowing by wire wrap spacers of thickness 2.24 mm. Detailed dimensions and parameters of the fuel pin and assembly are shown in Table III.

Boron carbide control rods will be used for the purpose of shutting down the reactor. Detailed design of these control rods has not been carried out yet. However, it is estimated that there will be 16 control assemblies, one between each toroidal field magnet. Since the control rods are 2 m in length and remain above the core during steady operation, additional design is required for the upper reflector, shield, and blanket regions.

III.D. Reprocessing

Pyrometallurgical reprocessing has been identified as the most appropriate means of reprocessing for the selected metal TRU-Zr fuel. This process is based on the use of high-temperature fused chloride salts to melt

TABLE III

Key Design Parameters of Fuel Pin and Assembly

Length of rods (m)	3.2	Total pins in core	248 778
Length of fuel material (m)	2	Diameter of flats (cm)	15.5
Length of plenum (m)	1	Diameter of points (cm)	17.9
Length of reflector (m)	0.2	Length of side (cm)	8.95
Radius of fuel material (mm)	2	Pitch (mm)	9.41
Thickness of clad (mm)	0.5	Pitch-to-diameter ratio	1.3
Thickness of Na gap (mm)	0.83	Total assemblies	918
Thickness of $LiNbO_3$ (mm)	0.3	Pins per assembly	271
Radius of rod with clad (mm)	3.63	Flow tube thickness (mm)	2
Mass of fuel material per rod (g)	241	Wire wrap diameter (mm)	2.24
$Volume_{Plenum}/Volume_{fm}$	1	Coolant flow area/assembly (cm^2)	75

the fuel, along with electrorefining techniques to separate the TRUs and fission products.[39,40] It was considered along with the aqueous PUREX reprocessing; however, pyroprocessing was deemed most appropriate. It has been shown to be especially suited for use with advanced fuels such as the TRU-Zr fuel employed here.[21,22,24] In the case of metallic alloy fuels, the PUREX process is more cumbersome and costly, since the irradiated fuel is brought from the metallic state to an aqueous solution, processed, and then converted again to metal through a number of reconversion steps. The pyrochemical reprocessing method, on the other hand, directly yields metal as the product.[41] A wider temperature range is available to amplify the differences in the thermodynamic stabilities that control the separation factors.[39,41] The ability to accommodate short-cooled and high-burnup fuels due to the higher radiation stabilities of nonaqueous reagents makes pyroprocessing especially suited for reprocessing of fast reactor fuels.

Proliferation resistance is one of the most attractive qualities of pyroprocessing.[39,41,42] The Pu is never separated from the highly radioactive minor actinides, which is important for proliferation resistance because the fission products are short-lived and their gamma contribution to 1 kg of TRU metal decreases to below self-protection levels 2 yr after being discharged.[39] Another attractive quality of pyroprocessing in terms of nonproliferation lies in that all of the reprocessing facilities can be located on-site, localizing problem areas, reducing diversion paths, and simplifying accountability.[40,42]

Pyroprocessing separates the spent fuel by means of high-temperature molten salts and electrolytic separation.[40] The metals in the fuel rod are dissolved in the high-temperature melt, then oxidized into chloride complexes. In the next process, the highly reactive metals are electrochemically deposited on the electrodes as voltage is applied.[43] Figure 7 shows a flow chart of the facilities involved in pyroprocessing

Pyrochemical reprocessing has been used only on a limited basis for making metal fuel for EBR-I and EBR-II. However, significant research and development has been performed at ANL (Refs. 21 and 27). At this time, there is no industrial-scale experience with metal fuel, pyroprocessing, or the reprocessing of fast reactor fuel. The following recovery rates, found in literature,[43] were used: Pu and Np 99.85%, Am 99.97%, and Cm 99.95%.

III.E. Fabrication

Fabrication of the TRU-Zr metal fuel will be accomplished through arc casting, which is a modified form of melt casting designed to allow the incorporation of actinides. Melt casting is currently used to fabricate plutonium and uranium metal rods and possesses numerous attractive qualities.[44] The process uniformly distributes the alloy so that the rods are homogenous and have identical compositions. Melt casting is very fast, with the actual casting of the fuel pins occurring in <1 s, and allows for hundreds of fuel rods to be cast at a time, which minimizes the time necessary to fabricate an entire batch of fuel.[44,45]

The primary concern when fabricating fuel with high actinide content is the susceptibility of low vapor pressure actinides to vaporization during the melting of the alloy and the transporting of the alloy throughout the furnace.[46] Using the standard casting method, americium loss of $>40\%$ has been measured.[47] Arc casting is

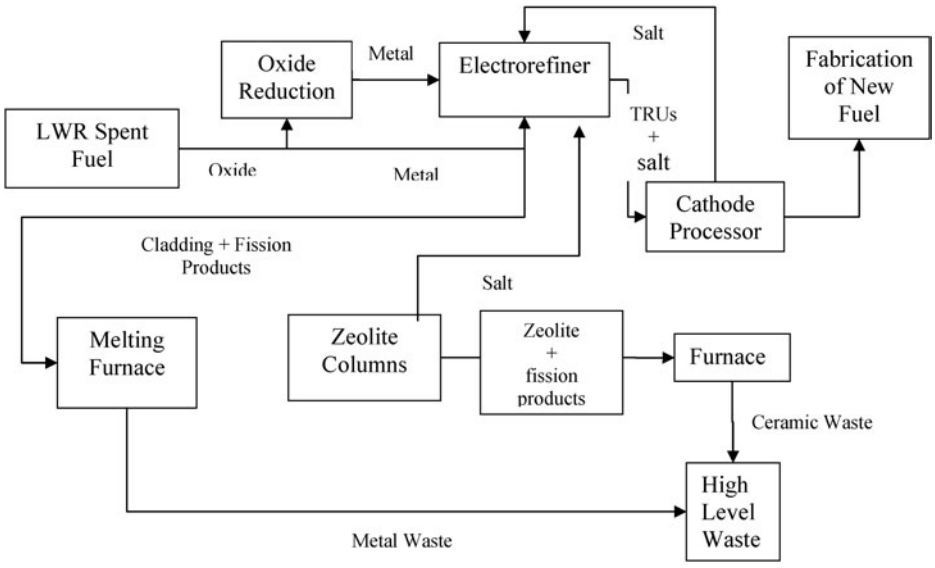

Fig. 7. Flowchart of pyroprocessing facilities.[43]

very similar to the standard melt casting method but with two alterations designed to minimize the loss of actinides to vaporization. Arc casting uses a low-voltage high-current arc to rapidly melt the alloy on the order of 5 to 20 s. This decreases the time to melt, and the actinides do not have enough time to escape.[21] Arc casting has been studied at ANL for 40Zr-10Am-10Np-40Pu fuel. Laboratory-scale tests have been done to test the ratio of the americium to zirconium content in the melt before casting and in the cast rods, and a ratio of close to one has been achieved.[48] Arc casting has been successfully completed at the laboratory level to fabricate rods for testing purposes, but the procedure is not believed to be reasonable for large-scale batches.

In order to maximize the throughput of transmutation fuel, the fabrication process will be automated. An automated process can be achieved by using commercially available equipment and constructing a hot cell. The hot cell would require robotic equipment and remote control and surveillance technology.[49] After casting, the rods would be mechanically sheared to the desired length, measured, weighed, and chemically analyzed. After filling the pin with sodium, the fuel rod will then be capped and welded shut. Integral quality control will be part of the production process.

The batch sizes may not contain more than 3 kg of TRU because of criticality concerns.[50] Casting and cooling the rods requires the longest time of any step in the cycle and is estimated to take 2 h, while the remaining fabrication steps should take under 2 h (Ref. 50). Assuming a facility down time of one-third with 24-h production, one facility could process ~8760 kg/yr. This is ~45% of the 20 t of TRUs that are produced annually by 100 GW(electric) of LWRs in the United States.[6,51] Using the proposed fuel dimensions, density, and compositions for SABR, there are 241 g of TRU per pin, which means 60 581 fuel pins could be produced annually. The initial fuel loading in SABR, which includes four batches of fuel, requires a total of 248 778 rods. Therefore, approximately four facilities based on arc-casting technology would be necessary to produce the fuel in a 1-yr time frame. New casting methods with larger batch size capabilities should be investigated. Induction casting may be a promising option. It is basically an extrapolation of the arc casting design. The method requires that the materials flow as solid materials and powders instead of as a molten alloy until they are quickly melted and cast.[52]

IV. NUCLEAR

IV.A. Neutronics Models

The fission core is an annulus, with dimensions given in Table I. The primary codes used to model the neutronics characteristics of this core were the multidimensional multigroup spherical harmonics code EVENT (Ref. 53) and the 3-D continuous-energy Monte Carlo code MCNP (Ref. 17). Due to the annular symmetry of the reactor, only a two-dimensional *r-z* model was used for EVENT. The CSAS sequences[54] were to create cross-section libraries for use in EVENT, and calculations were performed using a fifth-order (P5) spherical harmonic approximation and both the standard-scale 238-group energy structure and a reduced 27-group energy structure. This 27-group structure ranged from 0.1 meV to 20 MeV, with 20 fast groups above 10 keV. For the MCNP model, cross sections were generated using NJOY (Ref. 18) to Doppler-broaden the ENDF/B-VI.6 and ENDF/B-VII zero Kelvin libraries.[19] In the following sections, "beginning of life" refers to fresh TRU fuel in all locations, and "beginning of cycle" (BOC) and "end of cycle" (EOC) refer to the beginning and end, respectively, of the equilibrium fuel cycle in the in-to-out fuel shuffling scheme to be discussed in Sec. VI.

IV.B. Neutronics Properties

IV.B.1. Multiplication Constant

The SABR is designed to operate at a constant fission power level of 3000 MW(thermal). To compensate for the effects of burnup and fuel loading, the fusion power will be modulated as necessary to modulate the neutron source to maintain this power level. The fusion power required depends on the neutron multiplication of those source neutrons within the core. The fusion neutron source must be able to accommodate the associated decrease in neutron multiplication as the fuel is depleted. If M is the overall multiplication of source neutrons within the fission core, then $k_m = 1 - 1/M$ is the multiplication constant of those neutrons. Then, P_{fus} is given approximately by $P_{fus} = (E_{fus}/E_{fis})\nu(1 - k_m)/k_m \cdot P_{fis}$. For D-T fusion and actinide fission, $E_{fus} = 17.6$ MeV and $E_{fis} = 197$ MeV, and an effective ν was calculated by MCNP to be 2.98. For fresh fuel with $k_m = 0.95$, $P_{fus} = 42$ MW is required. Because the fusion neutron source can produce up to $P_{fus} = 500$ MW, the reactor can be operated with a k_m as low as 0.615.

IV.B.2. Energy Spectra

The neutron energy spectra are shown in Fig. 8 for BOC with all fresh fuel in all four core regions (see Fig. 2 for location) and in the tritium breeding blanket. The larger low-energy flux in region 1, closest to the fusion neutron source, is due to neutrons reflected from inboard of the neutron source across the plasma into the core.

IV.B.3. Control Rod Worth

Shutdown control of the reactor will be accomplished using a set of boron carbide control rods. As there are 16 gaps between the magnets of the SABR, it is

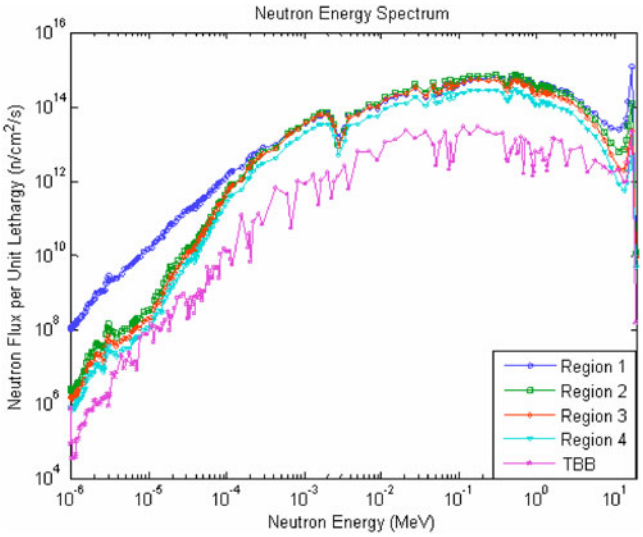

Fig. 8. Energy spectrum.

logical to use 16 control assemblies spaced evenly throughout the reactor. The removal of 16 assemblies of fuel material from the reactor causes <1% change in k_{eff}. The worth of 16 control rod assemblies, each with a B_4C mass of 10 kg, was calculated to be roughly 9 \$ ($\beta \sim 300$ pcm). Higher or lower overall worths can be easily accommodated if needed.

IV.C. Reactivity Coefficients

The Doppler and sodium voiding coefficients of reactivity are traditionally the most important in sodium-cooled fast reactors. The absence of ^{238}U in pure TRU fuel will tend to make the Doppler temperature coefficient less negative than in previous designs, or even positive, an effect which is offset somewhat by the zirconium matrix material in the fuel. The narrow tall annulus design of the SABR was chosen to maximize the negative leakage component of the sodium void worth.

IV.C.1. Doppler Temperature Coefficient of Reactivity

The EVENT code was used to calculate the Doppler coefficient, using data files generated in SCALE (Ref. 55). Cases were run every 100 K from an average fuel temperature of 535 K to 1135 K for the Doppler coefficient. A cladding temperature of 621 K and a coolant temperature of 600 K were used in all calculations. Cases were run for the beginning of life, where all fuel is fresh, and to the beginning and end of the equilibrium fuel cycle (see Sec. VI).

The Doppler coefficient $\rho/\Delta T = ((k_2 - k_1)/k_1 k_2)/\Delta T$ was calculated using the k_{eff} from EVENT for fuel temperatures differing by 100 K. For example, k_1 for the first point corresponds to 535 K and k_2 corresponds to 635 K, with $\Delta T = 100$ K, and the point is plotted at 585 K. The results are shown Fig. 9. The Doppler coefficients are very small, but generally negative, indicating the near cancellation of the positive contributions of ^{239}Pu and ^{241}Pu with the negative contributions of ^{240}Pu, the minor actinides, and the zirconium. Similar calculations made with MCNP, with cross sections Doppler-broadened using NJOY, yielded similar magnitude but positive Doppler coefficients; however, the statistical error was larger than the magnitude of the coefficient.

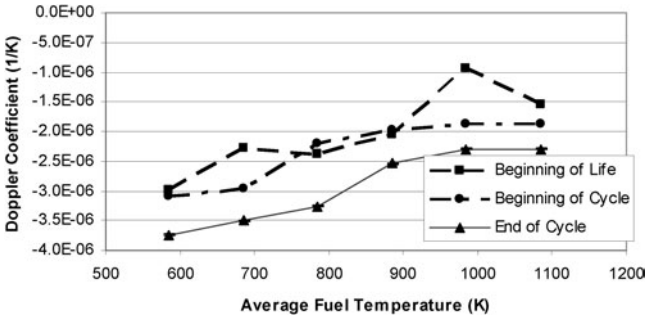

Fig. 9. Doppler coefficient versus average fuel temperature.

IV.C.2. Sodium Voiding Worth

The sodium density reactivity $\rho = (k_2 - k_1)/k_1 k_2$ was determined relative to the nominal density, where k_2 corresponds to the k_{eff} from EVENT corresponding to the reduced sodium density and k_1 corresponds to the k_{eff} for the nominal sodium density. These calculations assume a nominal average fuel temperature of 735 K, a nominal average cladding temperature of 621 K, and a nominal coolant and gap temperature of 600 K. The results are shown in Fig. 10. The sodium voiding worth is positive and approximately linear with decrease in sodium density.

An attempt to confirm these reactivity calculations using MCNP with cross sections processed using NJOY was unsuccessful because the statistical uncertainty in k_{eff} was too large.

IV.D. Tritium Production

The SABR design must be tritium self-sufficient with respect to fueling the D-T fusion neutron source. Lithium silicate was chosen for the breeding material because of its high lithium atom density and low probability of hydroxide formation, a safety consideration. Lithium has two naturally occurring isotopes, 93% ^7Li and 7% ^6Li, which has a large lower-energy (n,α) cross section. As indicated in Fig. 2, a natural lithium blanket was placed around the plasma neutron source and a blanket enriched to 90% in ^6Li was placed around the fission core.

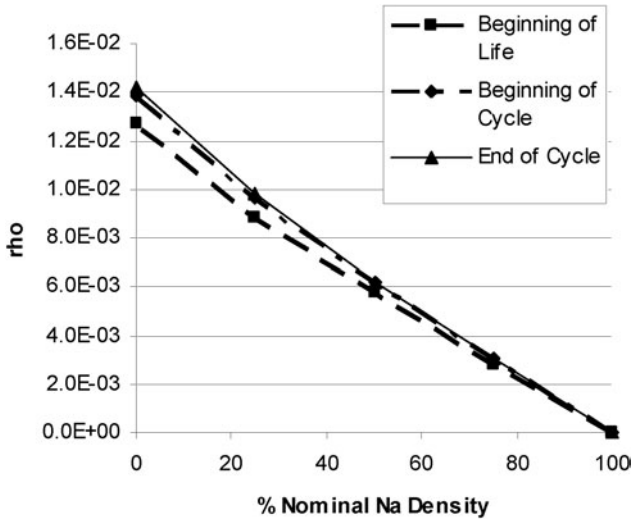

Fig. 10. Sodium voiding reactivity.

The requirement for tritium self-sufficiency over a nominal 750-day burn cycle, with enough excess tritium to start up the neutron source after a 60-day shutdown for fuel shuffling and to fuel it for one week into the next burn cycle, was taken as a design objective.

Previous experience[9] indicates that a tritium breeding ratio (TBR) (ratio of tritium production rate by neutron capture in lithium to fusion neutron source rate) of about 1.1 is sufficient to meet this requirement. The 27-group EVENT calculation of TBR, using cross sections generated with NJOY, yielded a TBR of 1.16.

An independent time-dependent tritium inventory calculation was performed with ORIGEN-S, using fluxes calculated by EVENT. This calculation indicated that the amount of tritium needed at the beginning of the burn cycle is 64 kg and that 69.8 kg of tritium would be present at this time.

IV.E. Shield Design

The purpose of the radiation shield is to attenuate the neutron and gamma radiation in order to limit radiation damage to the toroidal field magnets and to limit the activation of external reactor components to levels which permit personnel access within a reasonable period after shutdown. The maximum allowable dose limit[56,57] to the superconducting magnet insulators is estimated at 1×10^9 rads for organic insulators, and 1×10^{10} rads for ceramic insulators. The maximum allowable fast neutron fluence to the superconductor is in the range[57,58] of 5×10^{18} n/cm^2 to 1×10^{19}.

The shield was modeled using the Monte Carlo code MCNP (Ref. 17). The reactor module consisting of the core, plasma, tritium blanket, shield, fuel, and magnet was modeled as a series of cells bounded by right circular cylindrical surfaces, with the dimensions shown in Fig. 2.

The fusion neutron source was modeled as a volumetric, monoenergetic 14-MeV source. Calculation of the fluence and dose in the toroidal field magnets was based on an average volume tally for the area at the center of the inner magnet region where the fluence was the highest.

The first layer of the shield around the fission core (the tritium breeding blanket) contained a reflector region composed of ODS ferritic steel (Type 12YWT) and lithium silicate, which was used to reflect as many neutrons as possible back into the core region. Three layers of tungsten heavy alloy (Grade SDD185) were used to attenuate gamma photons and fusion neutrons, and a single layer of boron carbide was used as a thermal neutron absorber at the outside of the shield. Four sodium cooling channels were placed between each shielding layer to evacuate heat due to nuclear heating. The shield was designed to operate within the 500 to 800°C range. Table IV shows the arrangement of the shield layers from the inner to the outer region.

TABLE IV

Shield Layers and Compositions

Layer	Material	Thickness (cm)	Density (g/cm^3)
Reflector	ODS steel (12YWT)	16	7.8
Cooling channel A	Sodium-22	1	0.927
1	Tungsten heavy alloy (SDD185)	12	18.25
Cooling channel B	Sodium-22	1	0.927
2	Tungsten heavy alloy (SDD185)	10	18.25
Cooling channel C	Sodium-22	1	0.927
3	Boron carbide (B_4C)	12	2.52
Cooling channel D	Sodium-22	1	0.927
4	Tungsten heavy alloy (SDD185)	10	18.25

Basing the calculation on the maximum operating power level of 500 MW for the fusion neutron source and the 3000 MW(thermal) of fission power, it is calculated that the magnets will remain functional for their anticipated lifetime of 40 yr at 75% availability. Dose rate conversions were performed using ICRP-21 guidelines. The radiation limits[56,57] to the magnets are a fast (>0.1 MeV) neutron fluence of 10^{19} n/cm^2 in the superconductor and an absorbed dose in the insulator of 10^9 (10^{10}) rads for organic (ceramic) insulators. The calculated radiation for 40-yr operation at 75% availability are a fast neutron fluence of 6.9×10^{18} n/cm^2 and an absorbed dose of 7.2×10^7 rads.

V. THERMAL

V.A. Heat Removal

The core heat removal system will be a three-loop system, as shown in Fig. 11. The primary loop with liquid sodium coolant removes heat from the core and transfers it to an intermediate heat exchanger (IHX). An intermediate loop, with liquid sodium coolant, transfers heat from the IHX to the steam generator. The secondary loop converts the heat removed from the core to useful electrical energy.

The primary system is similar to other LMFBR designs, comprising core, IHX, piping, and sodium pumps. An intermediate sodium loop is employed for safety reasons, to separate the primary sodium from potential water ingress by tube rupture from the Rankine cycle. The secondary loop is a conventional Rankine steam cycle with a steam generator, turbine, condenser, and condensate pump. The steam generator provides superheated steam to drive the high-pressure and low-pressure turbines.

The mass flow rate through the core [3000 MW(thermal)] was calculated to be 8700 kg/s, with coolant T_{in} = 377°C and T_{out} = 660°C, and $c_{p,\mathrm{Na}}$ = 1.27 J/g K. The core power density is 73 MW/m^3. Coolant flow is upward through the core.

V.B. Fuel Pin Temperature Distribution

The quantities used to determine the temperature distributions of a fuel pin are linear heat rate; temperature of the coolant flowing into the core; and material properties of the coolant, cladding, and fuel. The thermal resistance equations[59] are used to calculate the temperate at the lithium niobate coating outside $T_{\mathrm{Li}O}$, Lithium niobate inside $L_{\mathrm{Li}I}$, cladding outside T_{co}, the cladding inside T_{ci}, the fuel outside T_{fo}, and the fuel centerline $T_{\max}$. The radius (R) and the conductivities[59] are given in Table V. The average linear heat rate q' was calculated[59] using $q' = Q/NL$, where Q is the thermal power deposited in the fuel pins, N is the number of fuel pins, and L is the active length of the fuel pins.

The clad-coolant heat transfer coefficient h was calculated from the Nusselt number Nu times the conductivity k of liquid sodium divided by the hydraulic diameter D_H. The Nusselt number was calculated using the Westinghouse correlation[59] $\mathrm{Nu} = 4.0 + 0.33(P/D)^{3.8}(\mathrm{Pe}/100)^{0.86} + 0.16(P/D)^{5.0}$, which is valid for pitch-to-diameter ratio of $1.1 \le (P/D) \le 1.4$ and a Peclet number of $10 \le \mathrm{Pe} \le 5000$. The Peclet number is the product of the Reynolds number and the Prandtl number.

The coolant temperature as a function of height along the fuel pin was calculated[59] using an inlet temperature of 377°C to ensure that the liquid sodium does not solidify.

The core thermal properties are summarized in Table V, and the nominal temperature distributions within a fuel pin are shown in Fig. 12. The temperature rise

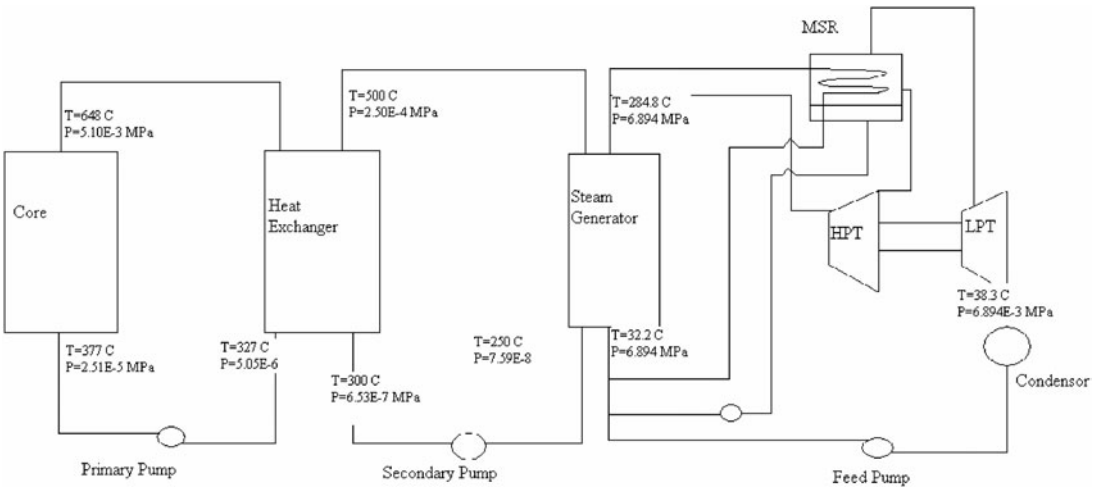

Fig. 11. Heat removal and power generation cycle.

TABLE V

Thermal Properties of Fuel Pin and Coolant

Conductivity of sodium (k)	6.26×10^{-5} MW/m·°C
Specific heat capacity (c_p)	1.27 kJ/kg·°C
Heat transfer coefficient (h)	0.05731 MW/m^2·°C
Nusselt number (Nu)	5.74
Reynolds number (Re)	28 700
Prandtl number (Pr)	4.63×10^{-3}
Average linear heat rate (q')	0.006 MW/m
Pitch to diameter (P/D)	1.3
Conductivity of cladding (k_c)	3.0×10^{-5} MW/m·°C
Conductivity of fuel (k_f)	1.0×10^{-5} MW/m·°C
Conductivity of gap (k_g)	0.00005 MW/m^2·°C
R_{co}	0.0033 m
R_{ci}	0.0028 m
R_{fo}	0.002 m
Flow area of core	7.5 m^2
Pump efficiency (η)	0.85
Density of sodium (ρ)	829 kg/m^3
Pressure drop (ΔP)	36 900 Pa
Electrical conductivity of the tube wall σ_s	1.10×10^{-9} $(\Omega m)^{-1}$
Electrical conductivity of the coolant σ_f	2.27×10^{7} $(\Omega m)^{-1}$
Conductivity of $LiNbO_3$ (k_{Li}) (Ref. 60)	0.0039 MW/m·°C

through the lithium niobate coating was found to be negligible.

V.C. Coolant Pumping

The conventional pumping power was calculated[57] using $P_{pump} = \Delta P \cdot \dot{m}/\eta \cdot \rho$ where ΔP is the pressure drop due to friction and gravity, $\dot{m}$ is mass flow rate, η is the pump efficiency, and ρ is the density of liquid sodium. The pumping power is 0.454 MW for the core.

A set of pumps moves the liquid sodium through the core and IHX. The factors affecting the pumping power are friction, gravity, and magnetohydrodynamic (MHD) pressure drop. The downside of using liquid sodium as a coolant for the reactor is the pressure losses that are experienced in moving sodium (a conductor) through the magnetic field that is in the core. This magnetic field is a result of the magnets that are needed for the confinement of the plasma in the fusion neutron source. When a conducting object is moved in a perpendicular direction to a magnetic field a current is introduced in the object. This current creates a Lorentz force that opposes the motion of the conducting material. The faster a conducting object is moved within the magnetic field, the larger the force that will oppose the motion of the object. This Lorentz force depends on $j \times B$, where j represents the current flowing in the sodium to the interfacing metal components and B is the magnetic field produced to confine the plasma in the fusion neutron source.

The Lorentz force can be represented[57] as an MHD pressure drop experienced by the coolant as it moves through the magnetic field: $\Delta p_{MHD} = L_C V B_\perp^2 \sigma_f C/(1 + C)$, where L_c is the distance that the coolant is pumped across, V is the velocity at which the coolant is pumped, and σ_f is the electrical conductivity of the coolant. The quantity $C = (2\sigma_s t/\sigma_f D)$, where σ_s is the electrical conductivity of the coolant tube wall and t is the thickness of the coolant tube wall. With the SABR parameters given above, the MHD pressure drop would be 68 MPa; this corresponds to a pumping power of 847 MW. This magnitude of pumping power is clearly excessive.

The current flow from the sodium coolant to the interfacing metal can be interrupted by coating the outside of the fuel clad and the assembly walls with a thin electrical insulator. The coating that was chosen for this purpose was lithium niobate.[60] Using lithium niobate as the insulator on all of the conducting surfaces that the sodium coolant will be flowing through allows the MHD pressure drop to be reduced to a negligible 2.48×10^{-6} Pa.

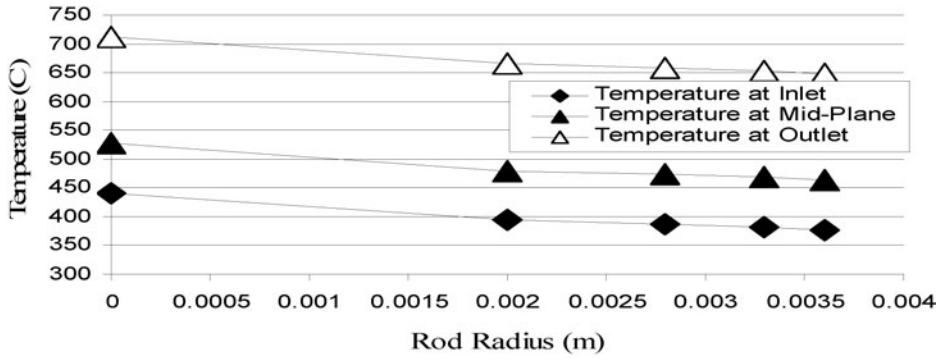

Fig. 12. Temperature distribution in fuel pin (fuel 0.0 to 0.2 cm, Na gap 0.2 to 0.28 cm, clad 0.28 to 0.33 cm, $LiNbO_3$ 0.33 to 0.36 cm).

TABLE VI

Core Thermal and Heat Removal Parameters

Power density	73 MW/m^3
Coolant T_{in}	377°C
Coolant T_{out}	650°C
Minimum centerline temperature	442°C
Maximum centerline temperature	715°C
Mass flow rate ($\dot{m}$)	8700 kg/s
Coolant velocity (v)	1.4 m/s
Total pumping power	454 kW

We note that compromise of the insulating layer due to cracking, corrosion, etc. could reestablish the Lorentz force locally, possibly leading to local flow reduction, flow redistribution, etc. Further research needs to be done on the effects of using lithium niobate in high-temperature sodium flows over long periods to determine how long it takes for its integrity to be compromised.

A summary of core thermal and heat removal parameters is given in Table VI.

V.D. Secondary Power Conversion Cycle

The SABR is designed to produce electricity, but without compromising its primary purpose of achieving a deep burn of TRUs. The secondary Rankine power cycle converts the steam into electrical energy. This cycle employs the use of a high-pressure and a low-pressure turbine in order to help maximize the efficiency of the cycle. Figure 11 gives the temperature and pressure for the critical points throughout the three-loop power conversion cycle. In the power generating loop, 10% of the steam exiting the steam generator is siphoned from the high-pressure turbine and is used in the moisture separator for reheat between the high-pressure and low-pressure turbine stages.

The power required to operate the heaters for the plasma and to operate the magnets is 120 MW. The power to operate all of the pumps throughout the three-loop system is 7.65 MW. (All of the calculations for the pumping power neglect the pressure losses due to the piping in the system; as a result, the required pumping power to operate this system will be higher than what was computed.) The total power produced by the turbine is 1049 MW(electric). This yields an overall thermal efficiency of 34.6% for the secondary power conversion system. The overall electrical efficiency of the system is 30.7%

V.E. Tritium Breeding Blanket Thermal Design

One of the design goals is tritium self-sufficiency, thus, a tritium breeding blanket surrounding the fusion and fission cores (see Fig. 2) is needed for tritium production. Within this blanket, neutrons interact with the breeding material, lithium silicate, and structure, giving rise to a corresponding nuclear heat generation.

This blanket must be cooled because of internal heat generation from the neutron flux. The temperature within the blanket must be kept between 420 and 640°C (Ref. 57) in order for online tritium recovery to be possible. It must be kept above 420°C so that the tritium produced in the lithium silicate microparticles will be able to diffuse to the surface of these particles. The lithium blanket must be kept below 640°C so that sintering and restructuring of the lithium silicate will be minimized. As sintering and restructuring occur the porosity of the lithium blanket would decrease, reducing the rate at which the tritium would be able to diffuse out of the blanket.[57]

The coolant chosen for the breeding blanket is liquid sodium, which is pumped through the breeding blanket in pipes of ODS steel in the configuration as depicted in Fig. 13. These pipes have a thin coating of lithium niobate, which reduces the MHD. In order to maintain the breeding blanket material immediately adjacent to the pipe within the temperature window, a gap of helium was placed around the main pipe structure using a double-wall configuration as shown in Fig. 13. The gap conductance was varied appropriately with respect to location within the blanket by variance of the pressure and density of the helium within the gap for different pipe sections. Channels of helium purge gas were also placed regularly throughout the blanket for tritium collection purposes (see Fig. 13), but were considered to be of negligible importance for cooling calculations because of low mass flow rates.

The power density used for the thermal design was estimated to be 3 MW/m^3 in the blanket next to the plasma neutron source first wall and to decrease exponentially into the tritium breeding region with an e-folding distance of 15 cm (Ref. 57). The power density at the outermost portion of the blanket was approximately half of the maximum power density and adjacent to the first wall. Only the cooling of that portion of the blanket surrounding the fusion core was considered in the thermal analysis.

A total of 2172 pipes of 1-cm diameter were used for cooling in the blanket, which removed 56.3 MW of power, the total power produced in the blanket surrounding the fusion core. The inlet coolant temperature for these pipes was 300°C, and the outlet coolant temperature varied with position in the blanket, the highest being 491°C. The temperature range in the blanket was found to be between 445 and 620°C, with the average blanket temperature being 533°C. The mass flow rate of coolant in the blanket was 650 kg/s, corresponding to a coolant velocity of 4.12 m/s. The pumping power required to cool the blanket surrounding the fusion core was found to be 35 kW.

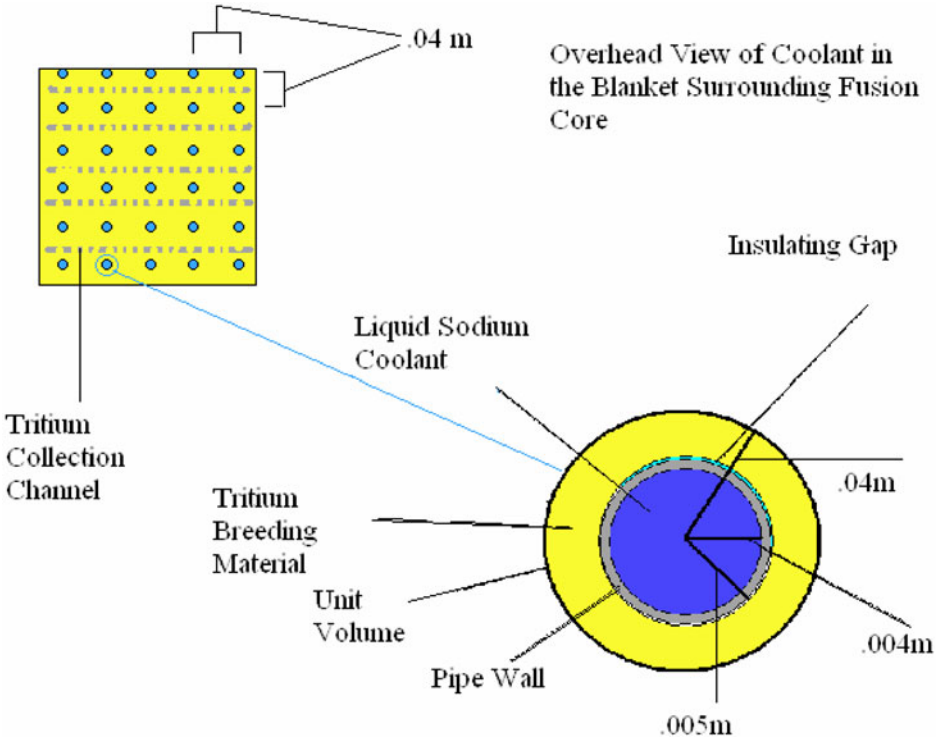

Fig. 13. Design of coolant in Li_4SiO_4 breeding blanket.

V.F. First Wall and Divertor

The fusion plasma neutron source is the same as developed for the design of the GCFTR transmutation reactor.[8–10] The plasma is capable of producing power up to 500 MW(thermal), 20% of which would be incident as a surface heat flux on the divertor and first wall of the plasma chamber. The thermal analysis on the fusion neutron source will be based on this maximum neutron source capability, even though the maximum neutron source requirement for SABR is only about one-half of this maximum capability (Sec. VI). This surface heat flux is assumed to be distributed with 50% on the annular plasma chamber and 50% on the divertor target plates. Some fraction of the remaining 400 MW(thermal) of power, which is in the form of 14-MeV neutrons, is deposited as a volumetric heat source in the first wall. The annular plasma chamber has a width of 2.16 m, a height of 3.67 m, and a centerline major radius of 3.5 m, which leads to a surface area of about 223 m^2.

V.F.1. First Wall

The first-wall design was adapted from the ITER design,[16] a beryllium-coated ODS structure, but with sodium instead of water coolant. The average surface heat flux at maximum fusion power [500 MW(thermal)] with 50% of the heat flux incident on the first wall is $\sim$0.25 MW/m^2. The first wall has been designed to allow for peaking and for 100% of the heat flux incident on the first wall, which leads to a design heat flux of 0.5 to 1.0 MW/m^2 for the first wall. This heat flux consists of the 20% of the fusion power plus the 98.2 MW(thermal) auxiliary power. The assumption for this design is that 10% of the first-wall surface area is unavailable since it constitutes the entrance to the divertor.

The first-wall design consists of a 3.5-cm-thick first wall between the plasma and the sodium coolant. For the sodium coolant paths, the dimensions are $\sim$4.5 m in length up each side of the first wall. The sodium is then removed from the system at the top of the first wall.

The first-wall temperatures are set for steady-state conditions at a range of 600 to 700°C and are limited to 1200°C in accident conditions, because of the melting point of the Be coating. Beryllium has a thermal conductivity of 200 $W \cdot m^{-1} \cdot K^{-1}$, and the ODS (Ref. 61) has a thermal conductivity range of 13 to 17.5 $W \cdot m^{-1} \cdot K^{-1}$. Using the thermal conductivities of the first-wall materials, the required flow rate of the sodium to cool the first wall to the temperature range of 600 to 700°C is 0.057 kg/s. This flow rate was calculated using the inlet and outlet temperatures set to 293 and 600°C, respectively. The first wall has a separate coolant loop, and the heat is not recovered for conversion to electricity. With this calculated flow rate, the use of an electrically insulating coating (lithium niobate) on the structure interfacing the

sodium coolant is required in order to prevent a large MHD pressure drop.

V.F.2. Divertor

The divertor design, based on the ITER divertor,[16,62] is plated with cubic tungsten tiles that measure 10 mm per side, as shown in Fig. 14. These tiles are bonded to finned CuCrZr layers behind which the sodium coolant flows. The coolant channels are located 4 cm from the plasma edge reaction with the tungsten tiles allowing for the maximum cooling capacity transfer to sodium without limiting the structural integrity of the tungsten or CuCrZr. The coolant channels have a 10-mm diameter and are coated in lithium niobate.

These cooling channels were designed along the width of the divertor in order to allow for the possibility of the cassette removal system chosen by ITER. The entire divertor design was modeled after the ITER design, except sodium was used rather than water coolant.

The divertor exhausts 50% of the heat flux leaving the plasma via the toroidal "target" strips below the plasma chamber. The heat flux impinging on the divertor is concentrated on two target strips measuring 0.8 m each in length. For these target strips, the estimated peak heat flux range is 1.0 to 8.0 MW/m^2. When compared with the ITER design,[62] which has about the same fusion power and a design heat flux range estimated to be less than 10 MW/m^2, the calculated values seem reasonable.

The heat flux impinging on the divertor was calculated the same way as described above for the first wall, with 50% of the maximum design power [500 MW(thermal)] from the plasma assumed incident on the divertor. Other factors affecting the heat flux include the fraction of exhaust heat flux radiated to the divertor channel wall and the heat flux peaking factor, which have been taken into account.

The divertor heat removal system was calculated analytically and modeled (following Ref. 10) using Fluent,[63] a 3-D fluid program that solves the energy equation coupled with the Navier-Stokes equation. The Fluent model and mesh were created in Gambit[63] for a single cooling channel. From this calculation the coolant flows at 1.22 m/s, flow rate at 0.09 kg/s, to keep the temperature of the CuCrZr at a maximum of 756°C with an inlet temperature of 293°C, both of which are well below the CuCrZr melting limit[64] of 1500°C.

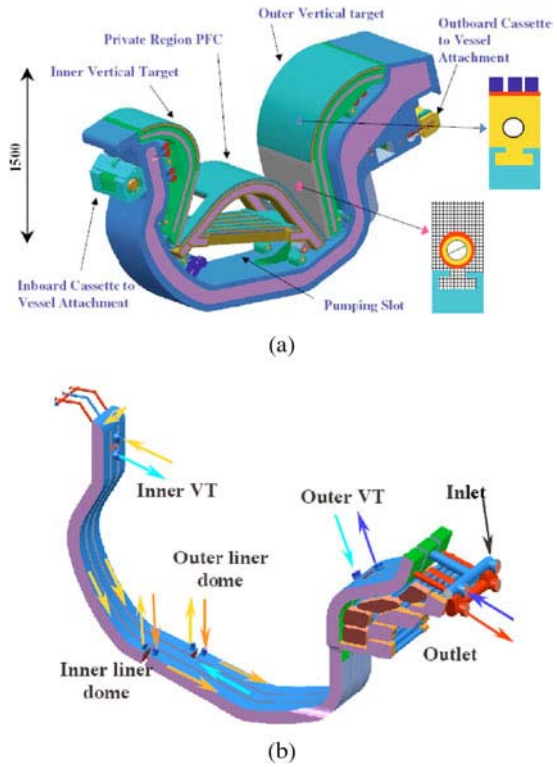

Fig. 14. (a) Divertor cassette[62]; (b) divertor coolant flow.[62]

VI. FUEL CYCLE

VI.A. Objective

The goal of the SABR is to achieve a deep-burn TRU burnup. The TRU, whose composition is given in Table VII, comes from LWR spent fuel. The primary objective is to reduce the actinide inventory in order to decrease the requirements on HLWRs. Previous studies[7–12] of subcritical transmutation reactors show that a deep burn is possible with either the use of a once-through cycle or using a fuel cycle that involves repeated reprocessing. This paper focuses on a fuel cycle

TABLE VII

TRU Fuel Composition in Number %

Isotope	Beginning of Life	BOC	EOC
^{237}Np	16.67	15.52	14.77
^{238}Pu	1.33	4.50	6.52
^{239}Pu	38.67	34.57	32.04
^{240}Pu	17.33	19.31	20.56
^{241}Pu	6.67	5.73	5.17
^{242}Pu	2.67	3.37	3.82
^{241}Am	13.83	13.33	13.00
^{242m}Am	0.00	0.18	0.32
^{243}Am	2.83	2.86	2.88
^{242}Cm	0.00	0.26	0.34
^{243}Cm	0.00	0.01	0.01
^{244}Cm	0.00	0.33	0.53
^{245}Cm	0.00	0.02	0.04

that involves repeated reprocessing. The burnup calculations in this paper are for the first cycle in a multicycle process. In order to accommodate a deep burn of TRUs, the fuel would be reprocessed and sent back through the SABR or another burner reactor.

VI.B. Methodology

In order to conduct the analysis, the EVENT (Ref. 53) and TRITON (Ref. 65) codes were used for the analysis. EVENT is used to determine the neutron flux and power distribution in the fission core. The power profile is then used to run a series of irradiation calculations with TRITON [ORIGEN-S (Ref. 66)]. After an irradiation step, updated number densities are used to regenerate cross sections (CSAS) that go into EVENT to recalculate the power profile. In order to use the cross sections from the SCALE package[55] for the fast spectrum in SABR, the 238-group cross-section library was collapsed to 27 groups using the 238-group energy spectrum calculated for SABR, which is a fast reactor spectrum with a 14-MeV tail.

Fuel batching and fuel shuffling were employed in the depletion of the fuel. The core was broken up into 4 annular equal volume regions (Fig. 3) so that the fuel is changed out after each burn cycle. For example in the in-to-out scheme, fresh fuel is loaded into the reactor and burned for 750 days, then the fuel in region 4 (outboard) is removed from the core, the fuel in region 1(inboard near plasma) is moved to region 2, the fuel in region 2 is moved to region 3, the fuel from region 3 is moved to region 4, and fresh fuel is placed in region 1 (inboard) and another 750-day irradiation cycle is carried out. The procedure is repeated until the equilibrium fuel cycle is reached: fresh fuel in the innermost region 1, once-burned fuel in region 2, twice-burned fuel in region 3, and thrice-burned fuel in region 4. Once this equilibrium fuel cycle is reached, each fuel batch is irradiated for four 750-day burn cycles. Each 750-day cycle contains six time steps at which number densities are updated and cross sections regenerated.

VI.C. Fuel Cycles

The fuel cycle design and analysis started by dividing up the reactor core into four equal volume annular regions, as depicted in Fig. 3. For the purposes of this analysis, each region was assumed to contain a uniform but time-dependent material composition throughout. Multiple shuffling patterns have been analyzed, though this report will focus on four such patterns: the out-to-in pattern, the in-to-out pattern, the region of high flux pattern, and the region of low flux pattern. This approach to the steady-state cycle is the same for all four cycles analyzed in the paper; the only difference is in how the fuel is shuffled.

Previous studies of subcritical transmutation reactors have shown that it is possible to achieve a deep burn of the TRU in a once-through fuel cycle,[10] provided that the reactor can be operated at a sufficiently low k_{eff}. To achieve this deep burn without reprocessing and recycling, a neutron source with the ability to produce 400 MW of fusion power was necessary. However, radiation damage accumulation to the clad and fuel assembly structure is estimated to limit the residence time for those components to somewhat more than 8 yr (Sec. IX), indicating the necessity to refrabricate the fuel after 8+ yr of irradiation. Therefore, this analysis looks at multiple fuel cycles of 3000-day length, with reprocessing and refabrication.

The power distribution is a function of both the fuel shuffle pattern employed and the length of the burn cycle. There are many factors involved that limit the fuel's residence time in the reactor and thus the burn cycle length:

1. Negative reactivity is introduced because of the fission product accumulation that comes along with the fuel depletion. This negative reactivity must be compensated for by the fusion neutron source.

2. The fuel pin plenum volume must be large enough to accommodate for the fission gases that are produced throughout the residence time without exceeding the material's strain limits.

3. Radiation damage to the clad must remain below the limiting value for the fuel pin failure.

4. The power peaking must not be excessive, where excessive was predicated here to be greater than 1.8.

Taking into account these factors as the limiting criteria, a fuel cycle with four burn cycles each of 750 days, resulting in a 3000-day residence time for the fuel, was chosen.

The power sharing among regions at the beginning of the equilibrium fuel cycle is shown in Fig. 15. Region 1 is inboard next to the plasma, and region 4 is outboard. No special effort (e.g., burnable poisons, within

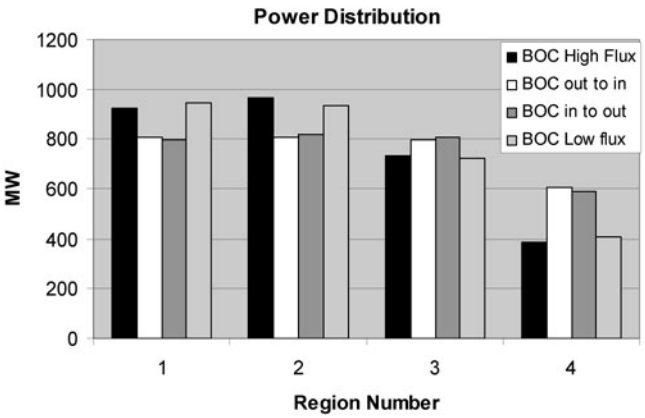

Fig. 15. BOC power sharing among fuel regions.

batch fuel zoning) has been made to flatten the power distribution.

At the BOC in the steady-state fuel cycle, fuel has been in the reactor for up to three residences (in region 4 for in-to-out), and one batch of fuel is fresh (in region 1 for in-to-out). The position of each level of burned fuel is dependent on which fuel shuffle pattern is being employed. In the in-to-out shuffling method, the most reactive fuel is in the innermost region of the core closest to the plasma, while the least reactive fuel is in the outer edge of the core. As the fuel is burned, there are two effects on the k_{eff} of the core, both introducing negative reactivity. First, the TRU (fissile material) is changed into fission products; second, neutron transmutation produces actinides with larger capture-to-fission ratio, such as ^{240}Pu and ^{242}Pu. These changes in the fuel are shown in Table VII for the in-to-out cycle operating with a batch burn cycle time of 600 days. These reactivity effects are taken into consideration when determining the length of the cycle, because not only do they influence the steady-state cycle but also the approach to the steady-state cycle.

The same 3000-day fuel cycle calculation described above for the in-to-out fuel cycle was carried out for the other three fuel cycle options: out-to-in, region of high flux, and region of low flux. Table VIII provides a comparison of the important fuel cycle parameters for each of the four fuel cycles analyzed.

Table VIII shows that in terms of burnup there is not a reason to choose one shuffling pattern over another. The out-to-in cycle shows greater burnup over the 3000 days, but this number is not much larger than the in-to-out or high flux. However, the power sharing among regions is more uniform for the out-to-in and in-to-out shuffling patterns, which have peaking factors of about 1.3, while the other two shuffling patterns have higher peaking factors up to 2.5. Primarily for this reason the in-to-out shuffling pattern was chosen for the SABR reference fuel cycle.

This reference 3000-day fuel cycle, limited by radiation damage to the fuel clad and fission gas pressure buildup, achieves 24 to 25% TRU burnup for the initial fuel cycle. Past experience[12] indicates that with reprocessing a >90% burnup can be achieved by recycling the refabricated fuel through the reactor about four times.

We note that cooling times before reprocessing, radioactive source levels during fuel fabrication, reprocessing losses, etc. can be as important for the overall assessment of the fuel cycle as the transmutation rate on which we have focused. A more detailed analysis of the equilibrium fuel cycle will be the subject of a future paper.

VI.D. Decay Heat

At the BOC, actinides within the fuel generate heat. As the fuel is burnt, decay heat from the fission products take over as the primary source of decay heat; therefore, decay heat generation in extensively burnt fuel is a major concern in thermal design for off-normal conditions in which coolant flow may be reduced or lost and must be accounted for in the primary heat removal system. If the heat removal system cannot adequately remove the decay

TABLE VIII

SABR Fuel Cycle Parameters

Parameter	Fuel Cycle			
	Out-to-In	In-to-Out	High Flux	Low Flux
Thermal power (MW)	3000	3000	3000	3000
Cycles per residence time	4	4	4	4
Burn cycle length time (days)	750	750	750	750
Four-batch residence time (yr)	8.21	8.21	8.21	8.21
BOC k_{eff}	0.88	0.89	0.89	.87
EOC k_{eff}	0.82	0.83	0.82	.81
BOC P_{fus} (MW)	109	99	99	119
EOC P_{fus} (MW)	175	164	175	187
TRU BOC loading (t)	36	36	36	36
TRU burned per yea (t/EFPY)	1.07	1.06	1.10	1.14
TRU burned per residence (t)	8.75	8.68	9.04	9.40
TRU burned per residence (%)	24.3	24.1	25.1	26.1
SNF disposed per year (t/EFPY)	96.3	95.4	99.0	102.6
Average core flux across cycle (n/cm^2·s)	2.80×10^{14}	2.88×10^{14}	2.69×10^{14}	2.92×10^{14}
Average fast (>0.1 MeV) flux (n/cm^2·s)	1.93×10^{14}	2.00×10^{14}	1.85×10^{14}	2.03×10^{14}
Fluence per residence time (n/cm^2)	7.26×10^{22}	7.46×10^{22}	6.97×10^{22}	7.56×10^{22}
Fast (>0.1 MeV) fluence per residence (n/cm^2)	5.00×10^{22}	5.18×10^{22}	4.79×10^{22}	5.26×10^{22}

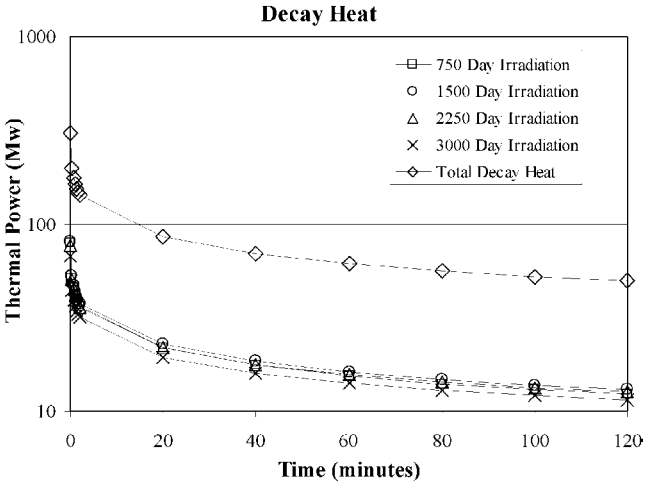

Fig. 16. Decay heat.

heat after the core has been shutdown, the entire reactor may be compromised. Ideally, a loss-of-coolant accident (LOCA) transient simulation should be run in order to ensure adequate removal of heat during an accident; yet, because of time constraints, the LOCA situation was interrogated analytically.

ORIGEN-S was used to calculate the thermal power from radioactive decay over time. Four different irradiation cases were used to accurately model the fuel composition in the core: 750, 1500, 2250, and 3000 days. The fuel was irradiated in the core for the previous cases and then allowed to decay for 2 h. The decay heat from all four cases was summed to give the total decay heat for a four-batch load. Data points were obtained for every 10 s up to 2 min and then subsequently for every 20 min up to 2 h after shutdown. Figure 16 shows decay heat initially at ~270 MW, ~9% of the total online power. Figure 16 also shows the decay heat leveling off at ~50 MW, or ~2% of the online power, which is consistent with standard decay heat schemes.

VII. DYNAMICS AND SAFETY

In order to design SABR to be passively safe, it is necessary to simulate the dynamic response to various off-normal conditions. This requires dynamic modeling of the three major coupled systems: the plasma neutron source, the reactor neutron population, and the heat removal systems. This coupled dynamics system, depicted in Fig. 17, can then be analyzed to determine if the inherent reactivity feedback mechanisms of the reactor are sufficient to shut down or limit the fission chain reaction in the event of a failure in one or more sections of the three coupled systems. The three major feedback mechanisms that affect the reactivity of the core are sodium

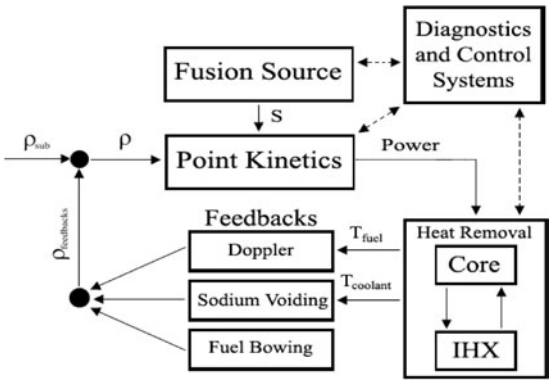

Fig. 17. Integrated reactor dynamics model.

voiding, Doppler, and fuel bowing. With reactivity feedbacks and the coupled dynamics model of the reactor, simulations of LOCAs, loss-of-heat-sink accidents, and loss-of-flow accidents (LOFAs) can be made. The diagnostic and control systems will be looked at in detail during future research.

VII.A. Fusion Neutron Source Model

The fusion model calculates dynamically the number of neutrons produced during the deuterium-tritium fusion reaction by solving the plasma ion and electron power balance equations,[67] taking into account ohmic, auxiliary, and fusion alpha heating and power losses due to radiation and transport, the latter based on the standard H98(y,2) energy confinement time correlation.[67] Coupled ion density balance equations[67] for the main and impurity plasma ions and the fusion alpha particles are solved.

The fusion neutron source rate is related to the fusion power production since each D-T fusion event produces 17.6 MeV, including one 14-MeV neutron. However, not all of the plasma neutrons reach the core. To calculate the percentage of fusion neutrons that reach the fission core, a calculation was performed with MCNP5 (Ref. 17). Of the neutrons created in the D-T fusion reaction, 39% are calculated to reach the fission core.

The fusion neutron source is designed to produce up to 500 MW(thermal) of fusion power. To operate at 500 MW of fusion power an external heating source of 98.6 MW is necessary.[10] Based on acceptable impurity limits in a plasma,[67] upper limits for carbon and tungsten were set at 3 and 0.008%, respectively, impurity atoms per ion.

VII.B. Neutron Kinetics

The point neutron kinetics equations[68] can be used to calculate the change in neutron and neutron precursor population as a function of reactivity and source strength.

TABLE IX

Delayed Neutron Precursor Variables for TRU Fuel

Group	Fresh TRU Fuel		Equilibrium TRU Fuel	
	λ (1/s)	Relative Yield	λ (1/s)	Relative Yield
1	1.324×10^{-2}	2.761×10^{-2}	1.324×10^{-2}	2.823×10^{-2}
2	3.019×10^{-2}	2.533×10^{-1}	3.019×10^{-2}	2.550×10^{-1}
3	1.166×10^{-1}	1.940×10^{-1}	1.166×10^{-1}	1.950×10^{-1}
4	3.133×10^{-1}	3.519×10^{-1}	3.133×10^{-1}	3.504×10^{-1}
5	1.046	1.376×10^{-1}	1.046	1.358×10^{-1}
6	2.836	3.553×10^{-2}	2.836	3.549×10^{-2}

Six groups of delayed neutron precursors were used, with delayed neutron fractions and decay constants determined for TRU fuel composition,[69] as given in Table IX. These changes in fuel and coolant temperature lead to changes in reactivity discussed in the following section.

The equilibrium condition is steady-state neutron and precursor population at $k_{eff} = 0.95$ (for the initial loading of fresh fuel), with reactivity $\rho = (k_{eff} - 1)/k_{eff}$, which is negative for a subcritical reactor, and a compensating neutron source S. The power density can be related to the neutron density in the core.

The one-group values for β and λ for the TRU composition for fresh fuel are 3.009×10^{-3} and 7.459×10^{-2}, respectively. For the equilibrium fuel composition, β and λ become 2.953×10^{-3} and 7.386×10^{-2}.

VII.C. Reactivity Feedbacks

The two obvious reactivity feedbacks for SABR are sodium voiding and fuel Doppler, as given in Sec. IV. Aside from these, there are fuel expansion and core expansion, which tend to be negative, and fuel bowing, which was positive and significant in EBR. The bowing reactivity was also examined. The time-dependent reactivity is then $\rho = \alpha_{\text{Doppler}} \Delta T_{fuel} + \alpha_{\text{Na}} \Delta N_{\text{Na}} + A_{bowing} + \rho_{sub}$, where ΔN_{Na} is the change in sodium density either due to a change in coolant temperature or to coolant voiding, ρ_{sub} is the subcritical reactivity (assumed constant), ΔT_{fuel} is the change in fuel temperature, and the Doppler and sodium density coefficients are proportional to the change in fuel temperatures and coolant density, respectively. The Doppler and Na voiding reactivity coefficients for SABR are given in Sec. IV, and the fuel bowing reactivity A_{bowing} is discussed below.

When a radial thermal gradient exists over the reactor, thermal deflections cause individual fuel rods to bow. The thermal deflection is caused because one side of the rod heats up and expands more than the other side. Assuming that the temperature gradient follows the neutron flux gradient, the motion of the bowed fuel is toward the higher temperature and neutron flux. This motion results in a positive reactivity gain A_{bowing} (Ref. 70). Bowing contributions are greatest when there is a substantial neutron flux and temperature gradient in the reactor radial direction. For a typical neutron flux distribution in the SABR, the average fuel temperature per region can be calculated. The temperature gradient is greatest in the fuel region farthest away from the fusion source. In this region an average temperature difference is between 2 and 3 K across opposite sides of a single rod.

For an individual rod, thermal deflections can be superimposed with force deflections imposed by the subassembly.[70] Figure 18 shows the calculated net deflections for a rod under 2, 5, and 10 K radial temperature gradients assuming that the structure is sufficiently rigid to fully constrain both ends of the rod. The deflection is in the direction of higher temperature and higher flux. In practice, the rods will not bow as much as shown in Fig. 18 because the wire wraps and spacer grids will be in place to mitigate the bowing toward the center.

To estimate the reactivity gain due to bowing, it is assumed that the bowing can be represented as a reduction in the volume of the reactor.[70] The reduction in volume means that the atom density of the fuel increases. The reactivity gain is then determined from EVENT neutronics calculations to be $\Delta k/k = -0.006 \Delta V/V$.

A radius reduction of 2 cm in the fuel region farthest away from the fusion source corresponds to a volume reduction of 3.08×10^{-3} m^3. This volume reduction gives a reactivity gain of $\Delta k/k = 0.0008$. A similar study for the EBR-I reactor calculated a much larger reactivity gain of $\Delta k = -0.35 \Delta V/V$. The EBR-I reactor is a much smaller reactor (volume < 0.01 m^3) than SABR; therefore, it is reasonable to expect that the EBR-I would be much more responsive to changes in volume due to bowing. According to Hummel and Okrent,[70] in a very large reactor whose fuel rods and subassemblies are constrained not to bow (by using spacer grids to hold the rods in place), the reactivity due to bowing should be negligible. Without physical constraints to prevent the bowing of the fuel rods, the reactivity gain due to bowing is expected to be positive but small.

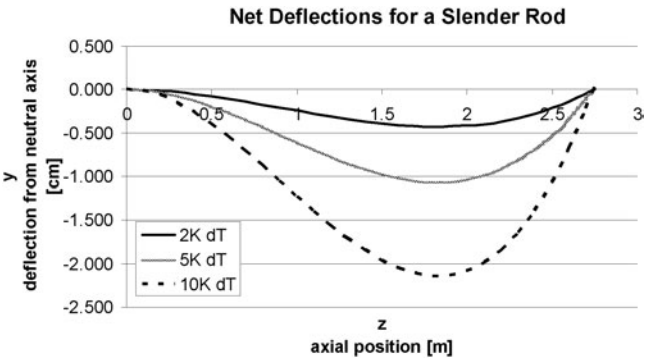

Fig. 18. Deflections for a fuel rod for radial temperature gradients of 2, 5, and 10 K.

VII.D. Heat Removal System

Modeling the dynamic temperature response is necessary to evaluate the safety of the temperature-dependent reactivity feedbacks. A two-temperature lumped model characterizes the entire reactor with an average fuel temperature and an average coolant temperature.[71]

The inlet coolant temperature $T_{c,inlet}$ is dictated by how much heat is removed through the IHX. At steady-state conditions, the heat removed from the hot side of the IHX equals the heat generated in the reactor. The IHX is approximated with an effectiveness that is a function of mass flow rate and inlet coolant temperature of the hot side loop (from the core). The effectiveness of a heat exchanger is the ratio of actual heat removed to the theoretical maximum heat removed[71]: $Q_{actual} = \varepsilon Q_{\max} = \varepsilon c_p \dot{m}(T_{Hot} - T_{Cold})$, where ε is the effectiveness and is calculated for a counter flow heat exchanger,[71] $c_p \dot{m}$ is the heat capacity rate of the hot side (primary loop), T_{Hot} is the coolant temperature entering the IHX from the core, and T_{Cold} is the inlet temperature on the cold side of the IHX. The average coolant temperature in the IHX is calculated from the heat balance on the IHX.

VII.E. Accident Analysis

An uncontrolled LOFA is modeled with no active shutdown of the plasma source or control rod insertion. To simulate a LOFA due to pump failure, the pumping power is decreased, which reduces the velocity of the coolant through the core. When the sodium pump malfunctions the mass flow rate is reduced and less heat is removed from the core, which leads to an undercooled reactor. This accident is initiated after 10 s of steady-state operation, when the pumping power is reduced instantaneously to a specified fraction of its original value. While reducing the pumping power instantaneously is not an accurate representation of a LOFA, it is a worst-case scenario and thus a conservative estimate of the accident.

Figure 19 illustrates the temperature response of the fuel during a LOFA. The first three accidents simulated are a 50, 75, and 85% decrease in pumping power, hence coolant velocity, through the core without any control action. The fourth accident is again a 75% decrease in coolant velocity, but now with the plasma neutron source shut down just prior to the time at which the sodium boils.

The limiting constraint to determine whether the reactor would suffer severe damage is the boiling point of the sodium coolant, which is 883°C. The fuel will melt at 1200°C, but in every LOFA case considered the sodium boiled prior to the fuel melting. It was determined that the coolant velocity through the core can be decreased by 71% (i.e., reduced to 29% of its original value) before sodium boiling will occur. (We note and will evaluate in a subsequent paper the possibility that a low melt point, ~750°C, eutectic might exist between the metallic fuel and clad and affect the accident progression.)

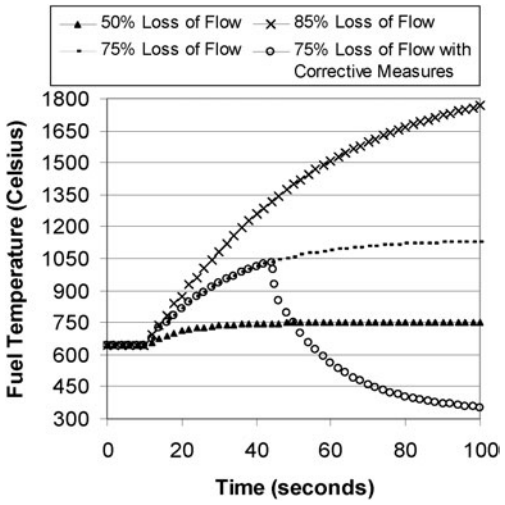

Fig. 19. Temperature response of fuel due to LOFA.

In the cases of the 75 and 85% decrease in coolant velocity through the core, there were 34.3 and 15.6 s, respectively, after the accident occurred before the sodium began to boil. This should be sufficient time to detect the loss of flow and to introduce control rods or shut down the plasma neutron source. The plasma neutron source can be shut down by shutting off the auxiliary heating power to the plasma, or by other means. For a LOFA, it was determined that if the plasma auxiliary heating system is shut down within ~1 s before the time at which sodium boiling otherwise would take place, the fission power will decrease enough that the coolant will not reach its boiling temperature and the fission power will eventually go to zero. This is illustrated in the fourth example in Fig. 19.

It should be noted that the temperatures discussed above are average temperatures, and as discussed in Sec. V the peak fuel and coolant temperatures will be ~40% higher. This will be examined in more detail, but probably will not change the general conclusion that about a two-thirds reduction in flow can be tolerated passively and that the time available to take control action is ample when larger flow reductions occur.

VIII. COMPONENT LIFETIMES

VIII.A. Fuel Pin

For liquid metal coolants such as sodium, the boiling point of sodium is not the limiting factor. The limiting factor is the creep lifetime characteristics of the primary system material, which are driven by the temperatures encountered by this material.[72] The thermal design must be balanced to avoid both the boiling of sodium and the failure of structural steel due to creep mechanisms. The nuclear design must also minimize power peaking to

TABLE X

EOC Plenum Gas Composition*

Helium	Bromine	Hydrogen	Iodine	Krypton	Xenon
2.03×10^{-3}	1.7×10^{-4}	9.33×10^{-5}	1.93×10^{-3}	2.66×10^{-3}	3.93×10^{-2}

*In moles.

reduce peak temperatures and cladding damage. Failure to accommodate the creep characteristics of structural materials will constrict fuel cycle time and increase cost, length, and frequency of outages.

Determining a strain and fatigue limit for structural components is an extremely difficult task because of the complexity of the behavior of materials in the radiation and thermal environments occurring in nuclear reactors.[72] For fast reactors, generally two specific mechanical limits have been used for fuel design. These limits are the strain limits and the cumulative damage fraction (CDF) method limit. For radiation damage, fluence limits are imposed. The fluence limits are produced by experimentation, through the observation of loss of mechanical strength after an average atom in the structural material has become displaced a certain number of times. Experiments have shown that irradiation has minimal effect on the creep strength of ferretic steel[33]; however, degradation of other mechanical properties can result from high neutron fluences.

The strain analysis method places a limitation on the diametrical growth of the clad. For preliminary study, limits of 2.0% total diametrial growth and 1.0% maximum thermal creep strain were imposed.[73] These are typical limits for fast reactor designs in the nuclear industry. The first cause of the diametrial growth is the thermal creep strain. Over the time period a fuel pin is in the core, deformation of the clad will occur because of strains resulting from the pressure of the gas plenum. For low smear density fuel pins, such as the ones proposed for the SABR, it can be assumed that the cladding strain can be determined solely with the plenum pressure stress. The extra room provided for the fuel slug to expand radially should prevent a significant fuel-clad mechanical interaction (FCMI). Because the strain is a function of plenum pressure, the size of the plenum may be extended to reduce the pressure buildup in the plenum. The plenum pressure was calculated using the ideal gas law, where the average numbers of moles of gas in a fuel pin was calculated using the ORIGEN code. Table X lists the composition of gases in the plenum after an average pin has been in the core for the 3000-day fuel cycle residence time. Because of the absence of data for fission gas release in the fuel slug, 100% of fission gas is assumed to immediately enter the plenum as it is produced. We use creep strain results from clad testing for MA957 performed by the DOE at Pacific Northwest National Laboratory[33] (PNNL). The pressure on the clad reaches its maximum, 11.1 MPa, at the EOC. Judging from comparison with the PNNL results, the creep strain should not exceed the limit of 1.0%.

Researchers at PNNL (Ref. 33) also observed void swelling for the MA957 cladding at fluences as low as 1.8×10^{22} n/cm^2. The researchers concluded that the swelling rate was expected to remain low at $<0.3\%$ per 10^{22} n/cm^2. With this strain limit approach, the SABR design appears to be acceptable, but a testing program will be required to confirm predictions.

Unfortunately, the strain limit approach to ensure fuel integrity has a deficiency in that the rupture strain is strongly dependent on the temperature and the strain rate.[72] To account for this, another method is used, the CDF method. This method assumes that damage to the clad occurs linearly and is determined through the use of a time-to-rupture correlation as a function of temperature and stress. The CDF is defined as follows: CDF = $\int_0^t dt'/t_r(\sigma, T)$, where t_r is time to rupture and t is the time in core (3000 days for a four-batch fuel cycle with 750-day burn cycles).[74] To be consistent with the strain analysis, the stress is assumed to be only the pressure in the plenum because of the low fuel smear density. A CDF value of 1.0 means that the clad would most probably fail at the end of the interval. This does not mean the clad will fail at the time that the CDF = 1, but that time is the average time to failure.[74] In 2000, mechanical and irradiation testing of the ODS steel MA957 was completed at PNNL. The time-to-rupture correlation found by PNNL (Ref. 33) was produced from biaxial tube rupture tests.

The CDF for SABR shown in Fig. 20 is calculated with the plenum pressure as a function of time used in this time-to-rupture correlation. The predicted average time to rupture (y-axis) remains well above the residence time in the core up to the design fuel cycle residence time of 3000 days.

The CDF limit is established by using statistical analysis from in-core experiments. To avoid an extensive and expensive test program, a statistical probability distribution function of failures from observed sample failures was used. Typically, no more than 0.01% of the fuel pins can be expected to fail, so the CDF limit is set using the probability distribution function to where there is a 99.99% confidence that no pin will fail.[72] Fuel pins using MA957 cladding have not been tested, but another experiment is

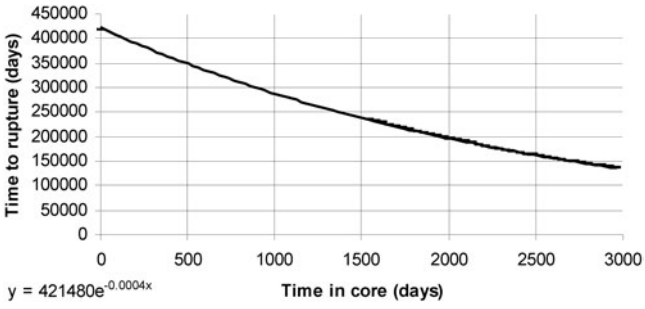

Fig. 20. Time to rupture for SABR fuel pin.

referenced for comparison. While EBR-II was in operation, the subassembly X447 was irradiated for testing. This subassembly contained uranium-zirconium fuel slugs with HT-9 cladding, similar to the SABR fuel pin design. To achieve a failure rate of less than 0.01% for this type of fuel, the CDF limit was 1.0% of the mean time to failure (CDF = 0.010) for the HT-9 clad without FCMI (Ref. 72). For the proposed 3000-day time-in-core for the SABR, the calculated CDF is 0.0136, or 1.36% of the mean time to failure.

VIII.A.1. Atomic Displacements

Component damage from atomic displacements caused by interactions with fast neutrons (>0.1 MeV) determine the expected lifetimes of various components of the SABR. The MA957 ODS cladding for the fuel pins is the main component of interest as it is the first line of defense against the release of the radioactive fuel and fission products. Using a damage limit of 200 dpa and a calculated average damage rate of 23.7 dpa/yr from a fast neutron fluence of 6.23×10^{22} n/cm^2, the clad will have an 8.44-yr lifetime. This means that from a radiation damage point of view, the clad radiation damage limit is consistent with the fuel cycle residence time of 8.21 yr.

The integrity of the TRU metal fuel is also a concern. Radiation damage to the fuel itself could limit the in-core time before reprocessing is necessary. Unfortunately, because the fuel is only recently under development, a dpa limit is unknown at this time. However, considering the composition of the fuel, most research suggests that the fuel should outlive the cladding in terms of radiation damage, and the cladding will serve as the limiting factor on the length of the fuel cycle.[75]

VIII.B. First Wall and Divertor

The first wall surrounding the plasma will be exposed directly to the 14-MeV fusion neutrons and hence accumulate more damage per neutron than the clad. At a fusion power of 500 MW, an effective full-power year (EFPY) produces a fast (>0.1 MeV) neutron fluence of 4×10^{22} (n/cm^2)/yr, which would in turn produce 33 dpa/yr. Assuming the same limit of 200 dpa for the ODS in the first wall, the first wall would need to be replaced every 6 EFPY if the fusion neutron source operated at its full design power of 500 MW. However, the fusion neutron source in the SABR design needs to operate at a variable power level much less than 500 MW (Sec. VI), and the first-wall lifetime would be correspondingly greater. It is plausible that the first wall could be replaced every two fuel cycles, or every 16.4 yr.

The divertor will require the most frequent replacement because of the damage it incurs from plasma erosion. Routine replacement will need to occur after every two burn cycles, or approximately every 4 yr; thus, considering a reactor lifetime of 30 EFPY, approximately eight replacements will need to be scheduled for the divertor.[76]

VIII.C. Superconducting Magnets

The Nb_3Sn magnets must be lifetime components for the SABR design to be feasible. The tungsten and boron-carbide shield (see Sec. IV.E) ensures that the maximum fast neutron fluence to the magnets never reaches the limiting value 10^{19} n/cm^2 during the design lifetime of 30 EFPY. The maximum calculated neutron fluence over 30 yr is 6.87×10^{18} n/cm^2, and the calculated dose to the epoxy insulator is 7.21×10^7 rads, which is lower than the limit of 10^9 rads.

IX. SUBCRITICAL OPERATION PROS AND CONS

Clearly, subcritical transmutation reactors with neutron sources will be more expensive and more complex than the same reactors operating critical. The advantages of subcritical operation must outweigh this added cost and complexity in order to justify such reactors. Realistic quantitative evaluation of the net benefit of these advantages will require a series of studies on comparative fuel cycle, safety, repository benefit, cost (of the reactors and the associated repositories), reliability, etc. We plan to undertake some such studies, but for now can only qualitatively discuss the probable issues.

High on the list of advantages postulated[3,4] for subcritical operation of transmutation reactors is safety. With pure TRU fuel the delayed neutron fraction β will be significantly smaller than with ^{235}U, and the absence of ^{238}U in the fuel will result in a much smaller negative (perhaps positive) Doppler reactivity coefficient, as found in this paper. Subcritical operation by an amount $\Delta\rho$ will increase the margin to prompt supercritical enormously from β to $\beta + \Delta\rho$, providing some flexibility to design around the safety challenges posed by TRU fuel in critical reactors. On the other hand, the absence of any known feedback mechanism to shut down the neutron source would certainly seem to be a drawback. Moreover, it has been argued that critical transmutation

reactors with significant ^{238}U in the TRU fuel could achieve almost as good net TRU destruction as with pure TRU fuel. Resolution of these issues will require comparative fuel cycle and safety studies, coupled with design studies to take advantage of unique features of both critical and subcritical reactors, scenario studies of required repository implementation, and cost and reliability studies.

Another advantage of subcritical operation is the added flexibility to achieve fuel cycles with deep burnup by compensating large burnup reactivity decrements with large neutron source strengths. Fusion neutron sources seem to have an advantage over accelerator neutron sources in this regard. For example, the neutron source for the SABR design was designed[10] to produce a maximum of 500 MW of fusion power, but the same design can produce less power (neutrons) by reducing certain operating parameters. Fuel cycle studies[10] of a gas-cooled transmutation reactor with the same 3000-MW(thermal) fission power output (hence transmutation rate) as SABR achieved equilibrium fuel cycle TRU burnups of 24.9, 49.7, 72.4, and 93.7%, with corresponding EOC k_{eff} of 0.927, 0.815, 0.714, and 0.611 and compensated EOC fusion neutron source powers of 73, 185, 286, and 389 MW(thermal), respectively, by adjustment of operating parameters. The longer burnups are associated with higher fast neutron damage rates, of course, and the maximum achievable burnup would be determined by structural failure.

Reliability and development needs of the neutron source are another issue. The neutron source design[10,77] used for SABR is based on the physics and technology database used for the ITER design,[16] thus, the development needs of ITER cover many of the development needs of the SABR neutron source, and ITER operation (beginning in 2016) will serve as a prototype for the SABR neutron source.

X. SUMMARY AND CONCLUSIONS

The conceptual design of a fusion-driven subcritical sodium-cooled transmutation reactor for high burnup, SABR, was described. SABR has an annular fission core surrounding the toroidal fusion plasma neutron source on the outboard side, with metallic fuel (Zr-Pu-Np-Am), a thermal power of 3000 MW(thermal), and an overall efficiency of 30.7% for electricity generation. The annular fission core contains 918 fuel assemblies, each holding 271 fuel pins with active length of 2 m. Sixteen of the assemblies contain enriched boron carbide rods, providing ~9 $ of negative reactivity. All structural materials and cladding are ODS steel.

A four-batch fuel cycle is used, with four burn cycles of 750 days, to fission the TRU in ~95 t of SNF each full-power year. Several fuel shuffling schemes were examined, with the somewhat surprising result that the flux and power profiles in the fission core are relatively insensitive to the fuel shuffling scheme. The reactor operates subcritical to achieve a deep-burn, four-batch fuel cycle which fissions 25% of the TRU in an 8.2-yr residence time, limited by radiation damage accumulation (200 dpa) in the ODS clad and structure. The discharged fuel would be reprocessed to remove fission products, refabricated, and recycled. The metallic fuel lends itself to pyroprocessing and is fabricated using arc casting to avoid release of volatile materials.

Reactivity coefficients were calculated and indicate that the Doppler coefficient of the fuel is small but negative (order of 10^{-6}/K), with increasing magnitude for higher burnup. The sodium void coefficient is always positive, but relatively small because of the high leakage annular core configuration (2 $ for 50% coolant voiding). The positive fuel bowing coefficient was estimated to be small both because of the size of the core and because of the spacing and wire wrapping of fuel pins.

A coupled core-neutron-kinetics plasma-source-dynamics lumped-parameter heat removal system model was employed to simulate the effect of LOFAs. Despite the positive Na-voiding reactivity, a significant reduction in flow (71%) can be tolerated passively, without shutting off the neutron source or inserting control rods, with no sodium boiling or fuel melting. For larger flow reductions sodium boiling would take place after tens of seconds, leaving ample time for corrective control actions. Simulations indicate that the plasma neutron source can be shut down rapidly in a controlled manner by reducing the auxiliary power to the plasma, such that initiation of source shutdown ~1 s before sodium boiling would otherwise occur is sufficient to prevent it.

A tokamak D-T fusion neutron source based on physics and technology that will be demonstrated in ITER supports the subcritical operation. The source would only need to operate up to 200 MW of fusion power, well below the 500-MW design limit based on ITER physics and technology. The SABR design is tritium self-sufficient due to tritium production in a lithium silicate tritium breeding blanket surrounding the plasma and fission core.

The magnetic field needed for the fusion neutron source poses a unique problem for the liquid metal coolant because of the large pumping power that would be required to offset the Lorentz force. However, this problem can be solved by coating all parts of the fission core and other structural parts in direct contact with the liquid sodium with an insulating layer of LiNbO, which virtually eliminates the current flow, hence the Lorentz force and the pumping power requirement. The shielding design limits the neutron fluence and radiation damage to the superconducting magnets so that these components do not need to be replaced during the reactor lifetime of 40 yr at 75% plant capacity factor.

The most important conclusions of this report are the following:

1. The SABR can achieve a high TRU burnup of ~25% FIMA in 3000 days of irradiation. The limit on the residence time in the core is set by 200 dpa material damage of the ODS clad and fuel assembly structural material.

2. The fusion neutron source strength required to compensate the reactivity decrement of 25% TRU burnup is 200 MW, well below the (ITER physics based) design level of 500 MW, which indicates that a fuel cycle with higher TRU burnup and larger reactivity decrement would be possible if the clad and structure damage limit can be extended beyond 200 dpa.

3. The annual TRU fission rate in SABR [3000 MW(thermal)] is comparable to the annual TRU discharge of three to five 1000-MW(electric) LWRs, depending on the plant capacity factor of SABR.

4. The time-scale for implementation of an ABR is 2020 to 2030, and the time-scale for implementing a fusion neutron source is 2030 to 2040, so SABRs could be implemented as part of a second generation of ABRs.

5. A single SABR can fission the discharged TRU from three 1000-MW(electric) LWRS. Thus, the HLWR requirements for a fleet of 1000-MW(electric) LWRs could be reduced by a factor of 10 to 100 by a fleet of SABRs in this 1:3 ratio.

6. SABR produces 921 MW(electric) of net power with an overall efficiency for power generation of 30.7%.

7. SABR is tritium self-sufficient.

8. The SABR Doppler reactivity coefficient is negative, the sodium void coefficient is positive, and both are small. Bowing of fuel rods is estimated to cause a negligibly small increase in reactivity.

9. Dynamic simulations indicate that an accidental reduction of flow up to approximately two-thirds can be tolerated (with no control action) without sodium boiling or fuel melting and that the time available for taking control action with larger loss of flow is on the order of tens of seconds.

Follow-up studies are in progress to provide an in-depth analysis of the fuel cycle and of the dynamic response of the coupled source-core heat removal system to off-normal conditions.

REFERENCES

1. U.S. Department of Energy's Global Nuclear Energy Partnership website; available on the Internet at http://www.gnep.energy.gov (2007).

2. "GEN-IV International Forum: Nuclear Energy Systems for the Future"; available on the Internet at http://www.gif.inel.gov/ (2007).

3. "First Phase P&T Systems Study: Status and Assessment Report on Actinide and Fission Product Partitioning and Transmutation," Organisation for Economic Co-operation and Development/Nuclear Energy Agency (1999).

4. *Proc. Int. Conf. Information Exchange Mtgs. Actinide and Fission Partitioning and Transmutation*, Mtgs. 1 through 9, Organisation for Economic Co-operation and Development/Nuclear Energy Agency (1990 through 2007).

5. NATIONAL RESEARCH COUNCIL, *Nuclear Wastes: Technologies for Separations and Transmutations*, National Academy Press, Washington (1996).

6. "A Roadmap for Developing Accelerator Transmutation of Waste (ATW) Technology," DOE/RW-0519, U.S. Department of Energy (1999).

7. W. M. STACEY et al., "A Fusion Transmutation of Waste Reactor," *Fusion Sci. Technol.*, **41**, 116 (2002).

8. W. M. STACEY et al., "A Subcritical, Gas-Cooled Fast Transmutation Reactor with a Fusion Neutron Source," *Nucl. Technol.*, **150**, 162 (2005).

9. W. M. STACEY et al., "A Subcritical, Helium Cooled Fast Reactor for the Transmutation of Spent Nuclear Fuel," *Nucl. Technol.*, **156**, 99 (2006).

10. W. M. STACEY et al., "Advances in the Subcritical, Gas-Cooled, Fast Transmutation Reactor Concept," *Nucl. Technol.*, **159**, 72 (2007).

11. E. A. HOFFMAN and W. M. STACEY, "Comparative Fuel Cycle Analysis of Critical and Subcritical Fast Reactor Transmutation Systems," *Nucl. Technol.*, **144**, 83 (2003).

12. J. W. MADDOX and W. M. STACEY, "Fuel Cycle Analysis of a Subcritical Fast Helium-Cooled Transmutation Reactor with a Fusion Neutron Source," *Nucl. Technol.*, **158**, 94 (2007).

13. R. N. HILL and H. KHALIL, "ATW System Point Design Employing Sodium Cooled Blanket Design," ATW Report, Argonne National Laboratory (2000).

14. W. S. YANG and H. KHALIL, "ATW System Point Design Employing LBE Cooled Blanket Design," ATW Report, Argonne National Laboratory (2000).

15. W. M. STACEY, "Tokamak D-T Fusion Neutron Source Requirements for Closing the Nuclear Fuel Cycle," *Nucl. Fusion*, **47**, 217 (2007).

16. ITER website; available on the Internet at http://www.iter.org (2007).

17. "MCNP: A General Monte Carlo N-Particle Transport Code, Version 5," J. F. BRIESMEISTER, Ed., Los Alamos National Laboratory (2003).

18. R. E. MACFARLANE and D. W. MUIR, "The NJOY Nuclear Data Processing System, Version 99," Los Alamos National Laboratory (1999).

19. M. B. CHADWICK et al., "ENDF/B-VII.0: Next Generation Evaluated Nuclear Data Library for Nuclear Science and Technology," *Nucl. Data Sheets*, **107**, 2931 (2006).

20. "Spent Nuclear Fuel Recycling Program: Report to Congress"; available on the Internet at www.gnep.energy.gov/pdfs/snfRecyclingProgramPlanMay2006.pdf (May 2005).

21. M. K. MEYER et al., "Development and Testing of Metallic Fuels with High Minor Actinide Content," Argonne National Laboratory (Apr. 20, 2003).

22. Y. SUZUKI, T. OGAWA, Y. ARAI, and T. MUKAIYAMA, "Recent Progress of Research on Nitride Fuel Cycle in JAERI," *Proc. Int. Conf. Fifth Information Exchange Mtg. Actinide and Fission Partitioning and Transmutation*, Mol, Belgium, November 25–27, 1998, Organisation for Economic Co-operation and Development/Nuclear Energy Agency (1998).

23. K. E. ABNEY et al., "Advanced Nuclear Fuel Processing Options Final Report," Los Alamos National Laboratory (Oct. 6, 1997).

24. S. HAYES and M. MEYER, Argonne National Laboratory, Personal Communication (2007).

25. "2002 Research Highlights: Technology Pioneered at Argonne Shows Promise For Next Generation of Nuclear Reactors"; available on the Internet at http://www.anl.gov/Media_Center/Frontiers/2002/d1ee.html (Apr. 23, 2007).

26. D. C. CRAWFORD, S. L. HAYES, and M. K. MEYER, "Current U.S. Plans for Development of Fuels for Accelerator Transmutation of Waste," Argonne National Laboratory (2000).

27. R. G. PAHL, E. L. PORTER, C. E. LAHM, and G. L. HOFMAN, "Experimental Studies of U-Pu-Zr Fast Reactor Fuel Pins in the Experimental Breeder Reactor-II," *Metall. Trans. A*, **21A**, 1863 (1990).

28. G. L. HOFMAN and L. C. WALTERS, "Metallic Fast Reactor Fuels," *Materials Science and Technology: A Comprehensive Treatment*, Vol. 10A, pp. 1–43, B. R. T. FROST, Ed., VCH Publishers Inc., New York (1994).

29. B. WILSHIRE and T. D. LIEU, "Deformation and Damage Processes During Creep of Incoloy MA957," *Mater. Sci. Eng. A*, **386**, 81 (2004).

30. E. YOSHIDA and S. KATO, "Sodium Compatibility of ODS Steel at Elevated Temperature," *J. Nucl. Mater.*, **329–333**, 1393 (2004).

31. M. K. MILLER et al., "Stability of Ferritic MA/ODS Alloys at High Temperatures," *Intermetallics*, **13**, 387 (2005).

32. S. UKAI et al., "Characterization of High Temperature Creep Properties in Recrystalized 12Cr-ODS Ferritic Steel Claddings," *J. Nucl. Sci. Technol.*, **39**, *8*, 872 (2002).

33. M. L. HAMILTON et al., "Fabrication Technological Development of the Oxide Dispersion Strengthened Alloy MA957 for Fast Reactor Applications," PNNL-13168, Pacific Northwest National Laboratory (2000).

34. B. O. LEE, W. S. PARK, Y. KIM, and T. Y. SONG, "The Preliminary Performance Analysis of the Transmutation Fuel for HYPER," *Proc. Int. Conf. Fifth Information Exchange Mtg. Actinide and Fission Partitioning and Transmutation*, Las Vegas, Nevada, November 9–11, 2004, Organisation for Economic Co-operation and Development/Nuclear Energy Agency (2004).

35. T. TAKIZUKA et al., "Accelerator-Driven Transmutation System Demonstration Experiments at JAERI," *Proc. GLOBAL '97*, Yokohama, Japan, October 5–10, 1997, Atomic Energy Society of Japan (1997).

36. A. L. PITNER and R. B. BAKER, "Metal Fuel Test Program in the FFTF," *J. Nucl. Mater.*, **204**, 124 (1993).

37. W. MARSHALL, *Nuclear Power Technology, Vol 1: Reactor Technology*, p. 316, Clarendon Press, Oxford (1983).

38. B. O. LEE, W. S. PARK, Y. KIM, and T. Y. SONG, "The Comparison of the Performance for the Alloy Fuel and the Inter-Metallic Dispersion Fuel by the MACSIS-H and the DIMAC," Korea Atomic Energy Research Institute (2002).

39. K. W. BUDLONG-SILVESTER and J. F. PILAT, "Safeguards and Advanced Nuclear Energy Systems: Enhancing Safeguardability," Los Alamos National Laboratory (Oct. 14, 2003).

40. "Report on the Preferred Treatment Plan for EBR-II Sodium Bonded Spent Nuclear Fuel," Office of Nuclear Energy, Science and Technology, U.S. Department of Energy (Oct. 2003).

41. D. BODANSKY, "Reprocessing Spent Nuclear Fuel," *Phys. Today*, **59**, 80 (Dec. 2006).

42. J. KANG and F. VON HIPPEL, "Limited Proliferation-Resistance Benefits from Recycling Unseparated Transuranics and Lanthanides from Light-Water Reactor Spent Fuel," *Sci. Global Secur.*, **13**, *3*, 169 (2005).

43. "Pyrochemical Separations in Nuclear Applications: A Status Report," Nuclear Energy Agency, Organisation for Economic Co-operation and Development (2004).

44. X. WU et al., "An Analysis of the Melt Casting of Metallic Fuel Pins," presented at U.S. Department of Energy's Quarterly Review Mtg., Albuquerque, New Mexico, January 22–24, 2003.

45. X. WU et al., "Design and Analysis for Melt Casting Metallic Fuel Pins," University of Nevada, Las Vegas (May 15, 2005).

46. Y. CHEN et al., "Phase I: Design and Analysis for Melt Casting Metallic Fuel Pins Incorporating Volatile Actinides," University of Nevada, Las Vegas (Nov. 15, 2002).

47. B. A. HILTON, J. R. KENNEDY, S. L. HAYES, and D. C. CRAWFORD, "Metallic Fuels for Actinide Transmutation," Presented at 9th OECD/NEA Information Exchange Mtg. Actinide and Fission Product Partitioning and Transmutation, Nîmes, France, September 25–29, 2006.

48. J. R. KENNEDY et al., "Characterisation of Actinide Alloys as Nuclear Transmutation Fuels," *Proc. 8th Information Exchange Mtg. Actinide and Fission Product Partitioning and Transmutation*, Las Vegas, Nevada, November 9–11, 2004, Organisation for Economic Co-Operation and Development/Nuclear Energy Agency (2004).

49. G. F. MAUER and J. RENNO, "Transmuter Fuel Fabrication: Design and Analysis of Robotic Manufacturing Processes," *Trans. Am. Nucl. Soc.*, **89**, 383 (2003).

50. G. F. MAUER, "Design and Evaluation of Processed for Fuel Fabrication: Quarterly Progress Report #3," University of Nevada, Las Vegas (Mar. 1, 2002).

51. F. VON HIPPEL, "Managing Spent Fuel in the United States: The Illogic of Reprocessing," available on the Internet at http://www.fissilematerials.org/ipfm/site_down/ipfmresearchreport03.pdf (Jan. 2007).

52. "U.S. Department of Energy Briefing on Advanced Fuel Cycle Initiative, AFCI," presented at 172nd Mtg. U.S. Nuclear Regulatory Advisory Committee on Nuclear Waste, Rockville, Maryland, July 20, 2006.

53. C. DE OLIVEIRA and A. GODDARD, "EVENT—A Multi-Dimensional Finite Element Spherical-Harmonics Radiation Transport Code," *Proc. Int. Seminar 3-D Deterministic Radiation Transport Codes*, Paris, France, December 2–3, 1996, Organisation for Economic Co-operation and Development (1996).

54. S. GOLUOGLU, N. F. LANDERS, L. M. PETRIE, and D. F. HOLLENBACH, "CSAS: Control Module for Enhanced Criticality Safety Analysis Sequences," ORNL/TM-2005/39, Version 5.1, Vol. I, Book 1, Sec. C4, Oak Ridge National Laboratory (Nov. 2006).

55. "SCALE: A Modular Code System for Performing Standardized Computer Analyses for Licensing Evaluation," ORNL/TM-2005/39, Version 5.1, Vols. I–III, Oak Ridge National Laboratory (Nov. 2006); available from Radiation Safety Information Computational Center at Oak Ridge National Laboratory as CCC-732.

56. L. A. EL-GUEBALY, "Shielding Design Options for the TF Magnets of ITER," *Proc. IEEE Thirteenth Symp. Fusion Engineering*, Knoxville, Tennessee, October 2–6, 1989, Institute of Electrical and Electronics Engineers (1989).

57. W. M. STACEY, *Fusion: An Introduction to the Physics and Technology of Magnetic Confinement Fusion*, Wiley-Interscience, New York (1984).

58. ITER General Design Requirements Document, S10 GDRD 2 95-02-10 F1.0, ITER (1995).

59. M. S. KAZIMI and N. E. TODREAS, *Nuclear Systems I: Thermal Hydraulics Fundamentals*, pp. 22–27, 295–338, 356–360, 450–451, Hemisphere Publishing Corporation, New York (1990).

60. L. KOVACS and K. POLGAR, "Electrical Conductivity of LiNbO3," *Properties of Lithium Niobate*, pp. 91–97, K. K. WONG, Ed., Institution of Engineering and Technology, Stevenage, United Kingdom (2002).

61. M. EL-GENK and J.-M. TOURNIER, "Mechanically Alloyed-Oxide Dispersion Strengthened Steels for Use in Space Nuclear Power Systems," available on the Internet at http://www.unm.edu/~isnps/online/presentations/MAODS.pdf (2004).

62. ITER, "Divertor"; available on the Internet at www.iter.org/divertor.htm (2004).

63. Fluent/Gambit, Version 6.1.22/s.1.2, "Computational Fluid Dynamics," Fluent Inc. (2004).

64. V. KOMAROV, A. LABUSOV, and A. MALKOV, "Acceptable Mechanical Properties of CuCrZr Cooling Tubes of ITER Divertor Plasma Facing Components," *Plasma Devices Oper.*, **10**, 17 (2002).

65. M. D. DEHART, "TRITON: A Two-Dimensional Transport and Depletion Module for Characterization of Spent Nuclear Fuel," ORNL/TM-2005/39, Version 5.1, Vol. I, Book 3, Sec. T1, Oak Ridge National Laboratory (Nov. 2006).

66. I. C. GAULD, O. W. HERMANN, and R. M. WESTFALL, "ORIGEN-S: SCALE System Module to Calculate Fuel Depletion, Actinide Transmutation, Fission Product Buildup and Decay, and Associated Radiation Source Terms," ORNL/TM-2005/39, Version 5.1, Vol. II, Book 1, Sec. F7, Oak Ridge National Laboratory (Nov. 2006).

67. W. M. STACEY, *Fusion Plasma Physics*, Wiley-VCH Verlag GmbH & Co. KGaA, Weinheim, Germany (2005).

68. W. M. STACEY, *Nuclear Reactor Physics*, John Wiley & Sons, New York (2001).

69. J. L. KLOOSTERMAN and J. C. KUIJPER, "VAREX, a Code for Variational Analysis of Reactivity Effects: Description and Examples," *Proc. Int. Topl. Mtg. Mathematical Methods for Nuclear Applications (M&C 2001)*, Salt Lake City, Utah, September 9–13, 2001, American Nuclear Society (2001).

70. H. H. HUMMEL and D. OKRENT, *Reactivity Coefficients in Large Fast Power Reactors*, American Nuclear Society (1970).

71. Y. S. TANG et al., *Thermal Analysis of Liquid Metal Fast Breeder Reactors*, American Nuclear Society, La Grange Park, Illinois (1978).

72. C. NAM, W. HWANG, and D. SOHN, "Statistical Failure Analysis of Metallic U-10ZR/HT-9 Fast Reactor Fuel Pin by Considering the Weibull Distribution and Cumulative Damage Fraction," *Ann. Nucl. Energy*, **25**, *17*, 1441 (1998).

73. A. E. DUBBERLEY, C. E. BOARDMAN, K. YOSHIDA, and T. WU, "Super PRISM Oxide and Metal Fuel Core Designs," *Proc. 8th Int. Conf. Nuclear Engineering (ICONE-8)*, Baltimore, Maryland, April 2–6, 2000, American Society of Mechanical Engineers (2000).

74. B. LEE and T. SONG. "The Preliminary Performance Analysis of the Metal Fuel for the Lead Cooled Critical Transmutation Reactor," *Proc. GLOBAL 2005*, Tsukuba, Japan, October 9–13, 2005, Atomic Energy Society of Japan (2005).

75. C. B. A. FORTY and P. J. KARDITSAS. "Uses of Zirconium Alloys in Fusion Applications," *J. Nucl. Mater.*, **283–287**, 607 (2000).

76. C. DAMIANI, "ITER Divertor Maintenance L7 R&D Project—Results and Perspectives," *Fusion Eng. Des.*, **51–52**, 925 (2000).

77. J.-P. FLOYD et al., "Tokamak Fusion Neutron Source for a Fast Transmutation Reactor," *Fusion Sci. Technol.*, **52**, 727 (2007).